Acta Biomaterialia xxx (xxxx) xxx



Contents lists available at ScienceDirect

Acta Biomaterialia

journal homepage: www.elsevier.com/locate/actbio



Full length article

Tumor proliferation and invasion are intrinsically coupled and unraveled through tunable spheroid and physics-based models

Ashleigh J. Crawford a,b,1, Clara Gomez-Cruz c,d,1, Gabriella C. Russo a,b, Wilson Huang b,e, Isha Bhorkar b,f, Triya Roy a,b, Arrate Muñoz-Barrutia a,d,g, Denis Wirtz a,b,f,h,*, Daniel Garcia-Gonzalez c,*

- ^a Department of Chemical and Biomolecular Engineering, Johns Hopkins University, 3400N Charles St, Baltimore, MD 21218, USA
- ^b Johns Hopkins Physical Sciences-Oncology Center and Institute for NanoBioTechnology, Johns Hopkins University, 3400N Charles St, Baltimore, Maryland 21218, USA
- ^c Department of Continuum Mechanics and Structural Analysis, Universidad Carlos III de Madrid, Avda. de la Universidad 30, 28911 Leganes, Madrid, Spain
- d Departamento de Bioingenieria, Universidad Carlos III de Madrid, Avda. de la Universidad 30, 28911 Leganes, Madrid, Spain
- ^e Department of Biology, Johns Hopkins University, 3400N Charles St, Baltimore, Maryland 21218, USA
- Department of Biomedical Engineering, Johns Hopkins University, 3400N Charles St, Baltimore, Maryland 21218, USA
- ^g Area de Ingenieria Biomedica, Instituto de Investigacion Sanitaria Gregorio Maranon, Calle del Doctor Esquerdo 46, Madrid' ES 28007, Spain
- h Departments of Pathology and Oncology and Sydney Kimmel Comprehensive Cancer Center, The Johns Hopkins School of Medicine, 1800 Orleans St, Baltimore, MD 21215, USA

ARTICLE INFO

Article history: Received 28 September 2023 Revised 13 December 2023 Accepted 26 December 2023 Available online xxx

Keywords: Tumor invasion Continuum model Mechanobiology Tumor growth

ABSTRACT

Proliferation and invasion are two key drivers of tumor growth that are traditionally considered independent multicellular processes. However, these processes are intrinsically coupled through a maximum carrying capacity, i.e., the maximum spatial cell concentration supported by the tumor volume, total cell count, nutrient access, and mechanical properties of the tissue stroma. We explored this coupling of proliferation and invasion through in vitro and in silico methods where we modulated the mechanical properties of the tumor and the surrounding extracellular matrix. E-cadherin expression and stromal collagen concentration were manipulated in a tunable breast cancer spheroid to determine the overall impacts of these tumor variables on net tumor proliferation and continuum invasion. We integrated these results into a mixed-constitutive formulation to computationally delineate the influences of cellular and extracellular adhesion, stiffness, and mechanical properties of the extracellular matrix on net proliferation and continuum invasion. This framework integrates biological in vitro data into concise computational models of invasion and proliferation to provide more detailed physical insights into the coupling of these key tumor processes and tumor growth.

Statement of significance

Tumor growth involves expansion into the collagen-rich stroma through intrinsic coupling of proliferation and invasion within the tumor continuum. These processes are regulated by a maximum carrying capacity that is determined by the total cell count, tumor volume, nutrient access, and mechanical properties of the surrounding stroma. The influences of biomechanical parameters (i.e., stiffness, cell elongation, net proliferation rate and cell-ECM friction) on tumor proliferation or invasion cannot be unraveled using experimental methods alone. By pairing a tunable spheroid system with computational modeling, we delineated the interdependencies of each system parameter on tumor proliferation and continuum invasion, and established a concise computational framework for studying tumor mechanobiology.

© 2023 The Author(s). Published by Elsevier Ltd on behalf of Acta Materialia Inc.

This is an open access article under the CC BY-NC-ND license (http://creativecommons.org/licenses/by-nc-nd/4.0/)

E-mail addresses: wirtz@jhu.edu (D. Wirtz), danigarc@ing.uc3m.es (D. Garcia-Gonzalez).

¹ Authors contributed equally

https://doi.org/10.1016/j.actbio.2023.12.043

1742-7061/© 2023 The Author(s). Published by Elsevier Ltd on behalf of Acta Materialia Inc. This is an open access article under the CC BY-NC-ND license (http://creativecommons.org/licenses/by-nc-nd/4.0/)

Please cite this article as: A.J. Crawford, C. Gomez-Cruz, G.C. Russo et al., Tumor proliferation and invasion are intrinsically coupled and unraveled through tunable spheroid and physics-based models, Acta Biomaterialia, https://doi.org/10.1016/j.actbio.2023.12.043

^{*} Corresponding authors.

Acta Biomaterialia xxx (xxxx) xxx

1. Introduction

Tumor growth can be broken down into a combination of cell proliferation and invasion [1,2]. When studying the tumor as a multicellular structure, these processes can be evaluated as the balance of cell proliferation, cell death, and nutrient access, which we term net tumor proliferation; and the balance of random cell migration, chemotaxis, and mechanical forces of migrating cells at the tumor boundary, which we term invasion. Some cancer cells detach from the tumor and invade the tissue stroma as single cells [3]; however, the tumor also invades the stroma as a cell aggregate, i.e., continuum invasion [4].

The interplays between net tumor proliferation, invasion, and the physical and mechanical properties of the tumor microenvironment (TME) make the mechanistic comprehension of tumor growth a challenging endeavor. For example, E-cadherin (E-cad), which is often expressed in breast cancer [5-9], decreases singlecell dissemination from a tumor via increased intercellular adhesion forces [10-13]. However, E-cad is also associated with worse clinical outcomes [14,15] and increased tumor proliferation [4]. In addition, breast cancer tumors remodel their microenvironment and deposit type I collagen [16-18], which significantly impacts the structural and mechanical properties of the extracellular matrix (ECM) [19-22]. The mechanical properties of a collagen gel do not always increase/decrease linearly with collagen concentration, and the elastic modulus, fiber alignment, and pore size cannot be independently tuned in vitro [19]. This paradoxical role of E-cad and the interdependent mechanical properties of a collagen-rich ECM contribute to the complicated dynamics of tumor growth.

In an in vitro tumor spheroid, E-cad expression and collagen concentration can be modulated to study their combined impact on net spheroid proliferation and spheroid invasion. We focus on invasion by the spheroid continuum in this work to study tumor growth independent of metastasis and the coupling of net proliferation and invasion within the cell aggregate. However, these experimental modulations cause multiple physical changes to the system, so computational models are required to isolate the individual consequences of each physical property. Previous in silico approaches aim to describe tumor growth with mathematical equations that integrate biochemical variables into physical governing equations. At the largest scale (multicellular), this problem is often modeled by continuum mechanics with formulations that divide the system's deformation into elastic and growth components [23,24], but the insights that can be obtained from a continuum approach at the tumor spheroid scale remain to be explored in the context of whole tumor growth. Such insights addressing the whole tumor provide valuable predictions of the mechanobiology of tumor evolution in a spheroid system that is commonly used for in vitro drug screening and studies of tumor biology [4,17,25].

Here, we suspended a dense cluster of E-cad- or E-cad+ MDA-MB-231 cells in 1-6 mg/mL type I collagen matrices using an oil-in-water droplet microtechnology [25]. Thus, E-cad expression and collagen density were adjusted in our tunable breast cancer spheroids to manipulate net spheroid proliferation and continuum invasion via both cell-cell and cell-ECM interactions. By embedding the spheroid core in matrices of excess ECM volume, we studied spheroid progression in a system where boundary effects were negligible. We observed increased net proliferation in E-cad+ spheroids and an inverse relationship between net proliferation and collagen concentration. Continuum invasion was also promoted by E-cad expression and limited by collagen concentration. System parameters and in vitro data were then integrated into a concise computational model. Using this model, we analyzed the influence of biomechanical parameters (spheroid stiffness, cell elongation, net proliferation rate and cell-ECM friction) on tumor progression from a continuum mechanics perspective. Spheroid growth is restricted by a limiting cell density of the system. This fixed variable regulates the maximum carrying capacity supported by the spheroid volume, total cell count, nutrient consumption rate, and collagen gel mechanical properties of each experimental condition. The maximum carrying capacity is observed through net proliferation and continuum invasion, but is determined by the biomechanical properties of the system.

2. Materials and methods

2.1. Cell culture

MDA-MB-231 shRNA transfection control (E-cad-) and E-cadherin lentiviral knock-in (E-cad+) as previously described [25,26] were maintained in Dulbecco's modified Eagle's medium (DMEM, Corning, 10,013-CV) supplemented with 10 % (v/v) fetal bovine serum (FBS, Corning, 35–010-CV), 1 % (v/v) Penicillin-Streptomycin (Gibco, 15,140–122), and 5 μ g/mL puromycin (Gibco, A11138–03). Cells were maintained at 37 °C and 5 % CO₂.

2.2. Spheroid culture

Spheroid cores were generated using the oil-in-water droplet technique [25] and 3D collagen I matrices generated following previously described protocols [19,27–29]. This system framework was adapted from Jimenez et al. [17]. Briefly, collagen I was prepared by thoroughly mixing equal parts cell culture medium (DMEM supplemented with 10 % fetal bovine serum and 1 % Penicillin-Streptomycin) and reconstitution buffer (1.1 g sodium bicarbonate and 2.4 g HEPES in 50 mL milli-Q water), then adding collagen I (Corning, HC Rat Tail, 354,249) to 1–6 mg/mL final concentration, and 1 M NaOH at a 4 % v:v ratio to the collagen volume. Cells were resuspended in collagen I at 1 \times 10⁴ cells/ μ L, and 1 μ L droplets gelled in oil columns for 1 hour at 37 °C. Cores were resuspended in bulk collagen I of the same concentration, and 100 μL of the mixture was plated in a preheated 96-well glass bottom plate (Cellvis, P96-1.5H-N) with one core centrally located in each well. The spheroid was incubated at 37 °C for 1 hour to allow the bulk collagen to gel before 100 µL warmed culture medium was added.

2.3. Spheroid imaging

Differential interference contrast (DIC) microscopy images of live spheroids were taken on days 1, 3, 5 and 7 using a Nikon A1R Confocal mounted on a Nikon Eclipse Ti inverted microscope and OKO Labs stage top incubator to control temperature and CO₂. Images were taken with a 10X/0.30 Plan Fluor objective, N1 DIC condenser and a 10X DIC slider (Nikon). GFP (488 nm) or RFP (561.5 nm) lasers were run concurrently with transmitted light. Images are 2048×2048 pixels with 2X line averaging.

Day 5 spheroids were fixed in 4 % paraformaldehyde (PFA, Sigma, 158,127) in DPBS (Corning, 21–031-CV) overnight at 4 °C. Spheroids were then washed 3X with DPBS and blocked using 5 % normal goat serum (NGS, Cell Signaling Technology, 5425) in DPBS for 3 h at room temperature. Spheroids were stained with 1:100 dilutions of primary antibodies (Cell Signaling Technology, Ecadherin 14,472, Ki-67 9449, Cleaved caspase-3 9661) in 1 % NGS in DPBS overnight at 4 °C. After 3X DPBS washes, secondary Alexa Fluor conjugated antibodies targeting mouse (ThermoFisher Scientific, A-11,004) and rabbit (ThermoFisher Scientific, A-21,245) were diluted 1:100 in 1 % NGS in DPBS to stain the spheroids for 3 h at room temperature. Spheroids were washed with DPBS 3X and cleared with fructose (Sigma, F0127)-glycerol (Promega, H5433) clearing solution [30]. Spheroids were imaged on a Nikon A1R Confocal mounted on a Nikon Eclipse Ti inverted microscope with a

Acta Biomaterialia xxx (xxxx) xxx

10X/0.30 Plan Fluor objective. Stacks of confocal microscopy images (10 μ m step size in the z plane) were collected at 1024×1024 pixels. Maximum intensity projections were produced using Fiji (ImageJ).

2.4. PrestoBlue viability assay

Spheroids were incubated in 1X PrestoBlue (Invitrogen, A13262) solution diluted in normal culture medium for 3 h at 37 °C. Blank wells prepared with 1X PrestoBlue were measured and subtracted from spheroid signals to account for background signal from the culture medium. A SpectraMax plate reader (Molecular Devices) was used to read the fluorescence intensity (Excitation 540, Emission 600, Cutoff 590). PrestoBlue readings on days 5 and 7 are reported as a fold increase from day of generation (day 0). Lee et al. has previously demonstrated that PrestoBlue readings linearly correlate to a cell count [25]. PrestoBlue measures the net proliferation rate of the spheroid and accounts for cell proliferation and death as a function of many system variables including nutrient consumption, depletion, and diffusion.

2.5. Image analysis

DIC microscopy images were corrected for illumination inhomogeneities and stitched using the ImageJ stitching plugin [31]. The spheroid continuum and detached cell regions were manually segmented for all replicates. We considered all individual cells or detached clusters of cells that present no contact domains with the spheroid continuum to be detached cells. Invasion distance from the spheroid continuum was defined as the mean of the minimum distance from all points at the outer edge of the detached region to the closest edge of the spheroid continuum.

Cell elongation was measured by segmenting all cells in a spheroid clockwise until at least 100 cells and a quarter of the spheroid had been segmented for each technical replicate. Cell circularity was calculated by the following equation [32]:

$$\mbox{\it Cell circularity} = 4\pi \left(\frac{\mbox{\it area}}{\mbox{\it perimeter}^2} \right)\!.$$

Cell elongation was calculated by:

Cell elongation = 1 - cell circularity.

An elongation value near zero means the cell morphology is rounded, whereas a value near one indicates that the cell is very elongated. To calculate the percentage of elongated cells in each condition, cells with an elongation score > 0.2 were considered elongated [33,34]. Normalized histograms of detached cell elongation were calculated for all conditions (E-cad expression, ECM collagen concentrations) on days 1, 3, 5, and 7 of spheroid growth. Cumulative histograms were calculated by counting all cells from the same conditions at all experimental time points. Image data analysis was performed using custom Python codes.

2.6. Continuum model

The tumor spheroid was conceived as a continuum cell aggregate to assess the spatial distribution of net proliferation and continuum invasion [35]. Here, we defined the cell aggregate as a continuum where local mechanical stimuli at the cellular level are globally transmitted in the form of mechanical waves and thus transport interaction forces throughout the cell continuum [36–39]. In parallel, local sources of cell proliferation increase the cell density, resulting in internal stresses within the continuum. These internal stresses oppose the external pressure from the ECM. The

mechanical balance between such internal and external forces governs the expansion of the cell aggregate. Capturing a complete formulation of cancer cell proliferation and invasion requires both the mechanical balance and the spatial evolution of cancer cell density. The variables of the problem are the displacement and cell density fields. The main parameters of the problem, along with their link to net proliferation and continuum invasion, are outlined in Table 1.

We assume negligible inertial effects for the mechanical balance, which is written in its spatial form as:

$$\nabla \cdot \boldsymbol{\sigma} + \boldsymbol{T} = 0, \tag{1}$$

where ∇ is the spatial gradient. The mechanical stress within the cell aggregate is described in its deformed state by the Cauchy stress tensor σ . The term T describes the external body forces.

The stress within the cell aggregate σ is defined by a constitutive equation which depends on the type of cancer cells modeled. The external body mechanical forces on the cell aggregate (T) are the result of cell-ECM interactions [40,41]. Therefore, we split these contributions between (i) cell-ECM friction that opposes spheroid invasion and (ii) propulsion forces exerted via cell-ECM adhesion that favor spheroid invasion:

$$T = -\zeta \, \mathbf{u} + f \, \mathbf{p} \tag{2}$$

where ζ is the friction coefficient, \boldsymbol{u} is the velocity field defined as the time derivative of the displacement field \boldsymbol{u} , \boldsymbol{p} is the cell elongation, and f is the magnitude of the propulsion body force (per unit volume).

We describe the evolution of local cell density ρ (defined as the number of cells per unit current volume) as the contribution of local proliferation sources, which depends on the limiting cell density ρ_{∞} , and a diffusion-like process mediated by an effective diffusion coefficient d:

$$\rho + \frac{J}{J}\rho = \nabla \cdot d\nabla \rho + g\rho \left(1 - \frac{\rho}{\rho_{\infty}}\right)$$
 (3)

where $J = det(\mathbf{F})$, with \mathbf{F} being the deformation gradient. The term g refers to the proliferation rate of cells per unit current volume. Note that the second term in the above expression accounts for the evolving spatial domain during proliferation, such that the mass balance is satisfied consistently [42,43].

The complete definition of the constitutive framework requires a constitutive equation for the cell aggregate stress (potentially linked to cell density) and the definition of the local proliferation source.

The definition of the mechanical behavior of the cell aggregate is formulated to provide a direct link between the mechanical stress within the cell aggregate and the cell density by making use of a multiplicative decomposition of the deformation gradient \mathbf{F} as [44–47]:

$$\mathbf{F} = \mathbf{F_e}\mathbf{F_p} \tag{4}$$

where F_e and F_p are the elastic and proliferation deformation gradient components, respectively. Note that the proliferation deformation is assumed volumetric and, therefore, the isochoric deformation (\vec{F}_e) is only related to the elastic component as:

$$\bar{\mathbf{F}}_{\mathbf{e}} = J^{-1/3}\mathbf{F} \tag{5}$$

The energy potential describing the mechanical response of the cells adopts a modeling scheme motivated by the neoHookean formulation as:

$$\Psi(\mathbf{F}, \mathbf{F}_{e}) = \frac{\mu_{s}}{2} \left[tr(\mathbf{\bar{F}}_{e}^{T} \mathbf{\bar{F}}_{e}) - 3 \right] + \frac{\kappa_{s}}{2} \left(\mathbf{J}_{e} - 1 \right)^{2}$$

$$(6)$$

where $J_e = det(\mathbf{F_e})$ is the elastic Jacobian. The parameters μ_s and κ_s are, respectively, the apparent shear and bulk moduli of the

Table 1Key parameters in spheroid proliferation and invasion dynamics.

Parameter	Definition			
Limiting cell density (ho_∞)	The limiting cell density of the system is the maximum number of cells per unit volume preventing further proliferation due to overrate of nutrients consumption and lack of physical space. This parameter is difficult to evaluate experimentally and, therefore, an important outcome of the modeling framework.			
Net proliferation rate (g)	The net proliferation rate of the system, which is influenced by E-cad expression. This variable is the net rate of cell proliferation and cell death including the consequences of oxygen/nutrient access. Note that net proliferation is not only determined by this variable, but also influenced by continuum cell invasion and its modulation by the limiting cell density. The three-dimensional friction experienced by cells when invading through the ECM. Therefore, this parameter strongly depends on the pore size of the collagen network which is determined by collagen concentration.			
Spheroid-ECM friction (ζ)				
Spheroid stiffness (κ_s)	The stiffness of the spheroid as a continuum. Under compression, it represents stiffness of the collective cell aggregate. Under tensile forces, it represents the mechanical resistance that a cell experiences when it tries to separate from the cell aggregate. E-cad expression permits the formation of adherens junctions, therefore influences the structural integrity of the spheroid as a continuum and modulates this parameter.			
Effective propulsion force (f_p)	The effective force exerted by the cells to invade the matrix. Such a cellular force is defined in a vector format with both a magnitude and direction. The magnitude is determined by the ability of the cells at the spheroid surface to propel themselves through the collagen fibers, dragging other cells from the interior of the spheroid. Therefore, this parameter is influenced by the ECM collagen concentration. Cell elongation determines how effective this force is. When the leading cells are highly elongated, cells invade more efficiently. Cell elongation can be obtained from the experimental results presented in Fig. 3 and depends on both E-cad expression and collagen concentration.			

cell aggregate (spheroid) describing the stiffness of the cell continuum or its resistance to deformation. Note that κ_s adopts different values depending on the stretch state. If $J_e < 1$, cells are under compression and this parameter refers to their material stiffness. Moreover, if $J_e > 1$, this parameter is determined by the intercellular adhesion governed by adhesion complexes and intermediate filaments. From thermodynamic principles the first Piola-Kirchhoff stress tensor can be derived as:

$$\mathbf{P} = \frac{\partial \Psi}{\partial \mathbf{F}} = \mu_s J^{-2/3} \left[\mathbf{F} - \frac{tr(\bar{\mathbf{F}}_e^T \bar{\mathbf{F}}_e)}{3} \mathbf{F}^{-T} \right] + \kappa_s (J_e - 1) J_e \mathbf{F}^{-T}$$
(7)

which is related to the Cauchy stress tensor by $\sigma = J^{-1} PF^T$. Note that the proposed framework allows us to define other complex constitutive equations by simply changing the conceptualization of the energy potential Ψ . Thus, an additive composition of Ψ can be used to add viscoelastic components (see Garcia-Gonzalez, D. & Landis, C. M., and Durcan, C. et al. [48,49] for consistent continuum visco-hyperelastic formulation).

Regarding the proliferation deformation gradient, it is directly linked to the current cell density as [50]:

$$\mathbf{F}_{\mathbf{p}} = \left(\frac{\rho}{\rho_o}\right)^{1/3} \mathbf{I} \tag{8}$$

where I is the second order unit tensor and ρ_0 is the initial cell density. Note that this constitutive choice assumes that the system is initially at an equilibrium cell density where the occupied space is equal to the summation of individual cell volumes. From a continuum perspective, if cells are adhered to each other, an increase in cell density under free stress conditions would cause a volumetric expansion of the system. Other alternatives may assume the initial state as a porous system so that an increase in cell density would result in densification with $F_p = I$ until reaching a density threshold [51]. Hence, the proposed formulation allows for densification of the system only if proliferation occurs within a mechanically constrained space. The consistency of the formulation under isolated invasion-proliferation cases is fulfilled by the intrinsic coupling of both processes.

Remark 1: Consider that the spheroid system is mechanically constrained, impeding volume changes (i.e., very high frictional terms). If the cells proliferate, local cell densities increase leading

to F_p undergoing volumetric expansion. However, the mechanical boundary conditions impede spheroid expansion, thus confining it so that F = I. According to Eq. (4), F_e will adopt volumetric compression values leading to internal compression states via Eq. (7). Hence, the formulation allows for mechanically constrained densification of the system until reaching its limiting cell density following Eq. (3).

Remark 2: Consider that cell proliferation is inhibited. Then, if the system invades driven by a propulsion force (independently of the magnitude of friction terms), the local cell densities will decrease as larger volumes are occupied by the same number of cells. Under such conditions, F presents volume expansion and F_p would adopt values lower than the unit following Eq. (3). Thus, $\vec{F_e}$ will adopt tensile deformation (i.e., volumetric expansion) leading to tensile stresses within the spheroid, consistent with the problem simulated. The proposed model aims to capture the essential mechanics driving invasion and proliferation interplays while reducing the number of model parameters to calibrate. The formulation could be extended to include nutrient/oxygen diffusion and its related impact on proliferation and cell death within the continuum framework. This consideration would result in a spatial heterogeneity of cell proliferation leading to an inert necrotic domain within the spheroid center. However, its implementation would require further experimentation measuring species diffusivities depending on collagen concentration. To avoid ad-hoc fitting of these parameters, our first simulations assume a constant cell proliferation rate. We later incorporate an estimated linear and exponential distribution of cell proliferation rates in the model to simulate these anticipated effects. Experimentally, we measure a cumulative cell proliferation/death (net spheroid proliferation) for all spheroid conditions and image representative distributions of cell proliferation (Ki-67) and apoptosis (Cleaved caspase-3) to justify these assumptions. Note that these assumptions only affect proliferationinduced invasion, as the contribution of active invasion (propulsion force) is modulated by cell elongation, which is 0 in the inner region of the spheroid in any case.

2.7. Calibration and motivations of model parameters

The model is designed to isolate intercellular and extracellular mechanical properties in a simplified manner considering the cell

Table 2 Motivation for parameter values for model calibration.

Parameter	Calibration			
Limiting cell density (ho_∞)	This value is calibrated for the reference case (E-cad+, 4 mg/mL collagen) and kept constant for all conditions.			
Net proliferation rate (g)	This parameter is influenced by E-cad expression [4] and can be extracted from the experimental data. Note that this parameter is kept constant for all extracellular conditions. This parameter is directly linked to the pore size of the collagen matrix. It cannot be measured experimentally, so we first calibrate the friction term for the reference case (4 mg/mL). Then, the friction coefficient for the different extracellular conditions is determined by an inverse relation with the pore volume of the surrounding collagen, so no fitting is used. This relation was determined in a previous work by the authors (Supplementary Figure 8) [19]. This work measured the pore size of collagen gels ranging from 1 to 6 mg/mL. Therefore, this spheroid-ECM friction parameter decreases with collagen concentration where the average pore size is larger.			
Spheroid-ECM friction (ζ)				
Spheroid stiffness (κ_s)	This parameter is related to the mechanical resistance of the spheroid. Under compressive forces, this parameter is the cell stiffness [63–65]. Under tensile conditions, it is the force needed to detach cells. Adhesions between cells cause resistance to cell detachment, so this parameter is defined by E-cad expression. Stiffness is the ratio of the mechanical stress before cell detachment to the corresponding strain. Note that this strain considers two adhered cells as a continuum. The experimental data for E-cad-/+ conditions were taken from a previous work by the authors [67]. The stress is the force needed to separate two cells divided by the cross-sectional cell area, so the net force is the force of one E-cad/E-cad bond multiplied by the average number of bonds between two cells. Note that absent E-cad will reduce both the number of bonds and their strength. Therefore, spheroid stiffness in both E-cad+ and E-cad-conditions was experimentally measured without ad hoc fitting.			
Effective propulsion force (f_p)	This parameter is defined by two variables: the propulsion body force and the cell elongation. The propulsion body force is kept constant for all conditions and estimated by the force per individual cell, approximately 10^2-10^3 nN in magnitude [80]. Therefore, the propulsion body force per unit volume in the spheroid can be computed as the force exerted by a single cell multiplied by the cell density. We considered the initial cell density of our spheroids for this approximation. Cell elongation was measured experimentally (Fig. 3, Supplementary Figure 1C-D, Supplementary Figure 5). Under E-cad+ conditions, where cell-cell adhesion is strong, we assumed a linear distribution of the elongation to zero from the leading edge to the center of the spheroid. For E-cad- conditions, intercellular adhesion is weaker, which results in easier detachment of the leading cells from the continuum and reduced force transmission. For this case, the propulsion force was modeled as a steep exponential function where only cells very close to the edge have a non-negligible propulsion force.			

Table 3Constitutive parameters used in the simulations.

2 mg 8 ·		$g (s^{-1})$ $1.95 \cdot 10^{-6}$) $4 mg/mL$ $2.65 \cdot 10^{4}$	f (N/mm ³) 0.6 6 mg/mL 5.46 · 10 ⁴		
2 mg 8 ·	g/mL	4 mg/mL			
8 -					
(
·	ell elongation (p)				
1 mg/mL	2 mg/mL	4 mg/mL	6 mg/mL		
0.320	0.412	0.357	-		
0.171	0.166	0.240	-		
Value adju	stment for E-cad expres	sion			
$\kappa_s^{tension}$ (kPa)		g (s ⁻¹)			
$0.143 \ 0.10^{-6}$			$1.95 \cdot 10^{-9}$		
	Cell density				
ρ ₀			$ ho_{\infty}$		
	1 mg/mL 0.320 0.171 Value adju tension (kPa) 143 0·10 ⁻⁶	1 mg/mL 2 mg/mL 0.320 0.412 0.171 0.166 Value adjustment for E-cad expression (kPa) 143 0·10 ⁻⁶ Cell density	1 mg/mL 2 mg/mL 4 mg/mL 0.320 0.412 0.357 0.171 0.166 0.240 Value adjustment for E-cad expression tension (kPa) g (s ⁻ 1.43 0·10 ⁻⁶ 1.95 · Cell density ρ ₀ ρ ₀		

aggregate as a continuum. We first calibrated the model parameters using a spheroid condition that expressed E-cad (E-cad+) and a collagen concentration of 4 mg/mL as a reference. In this condition, invasion was limited by large frictional forces, so the limiting cell density (ρ_{∞}) could be determined.

Then, all experimental modulations to model parameters were determined based on experimental data without further fitting. We present the motivation for each choice in Table 2.

The model parameters used in the simulations are collected in Table 3. Note that the diffusion coefficient is kept constant to not influence proliferation and invasion between the tested conditions.

This variable represents the tendency of cells to occupy regions of lower cell density.

2.8. Statistical methods

Statistical analyses are listed in the figure legends with p-values (**** $P \le 0.0001$, *** $P \le 0.001$, ** $P \le 0.01$, ** $P \le 0.05$), error bars, and replicate information (N =biological replicates, n =technical replicates). Statistical comparisons are unpaired t-tests or twoway ANOVA with multiple conditions. Additional information for all statistical tests is provided in the Supplementary Data excel

Acta Biomaterialia xxx (xxxx) xxx

file where all p-values are provided in heatmap format. In these heatmaps, green is P \langle 0.0001 and red is P \rangle 0.9999. GraphPad Prism was used for most of the statistical analysis. Proliferation data was normalized with respect to the initial number of cells (10,000 cells/spheroid core) on the day of spheroid generation (day 0), and invasion data was normalized with respect to the cross-sectional area of each spheroid after spheroid generation (day 1). The initial cell count and spheroid core volume were constant for all experimental conditions.

3. Results

3.1. Net spheroid proliferation and invasion are manipulated in a tunable spheroid system

3.1.1. Net spheroid proliferation is promoted by E-cad and limited by collagen

This work explores the influence of intercellular and extracellular mechanical conditions on the multicellular proliferation and invasion of tumor spheroids. To manipulate these two phenotypes, we experimentally modulated cellular expression of adhesion molecule E-cad and ECM collagen concentration. Together, these spheroid parameters alter the net proliferation rate of the tumor spheroid, and the intercellular and cell-ECM mechanical interactions within the system. To this end, we studied MDA-MB-231 breast cancer cells, which do not endogenously express E-cad (E-cad-), and MDA-MB-231 cells that express E-cad via lentiviral knock-in (Ecad+) [26]. The mechanical properties of the ECM were controlled by seeding spheroids in collagen I gels at concentrations between 1 and 6 mg/mL. Our spheroid system utilized the previously reported oil-in-water droplet microtechnology [25] to enclose E-cad- or E-cad+ MDA-MB-231 cells in an inner collagen I compartment, which we term the spheroid core (Fig. 1A). This spheroid core was suspended in a 100X larger collagen I matrix of the same concentration (Fig. 1A).

E-cad expression regulates intercellular mechanics through adherens junctions [52,53] that favor spheroid invasion as a continuum and promote net spheroid proliferation [4] (Fig. 1B). Ecad is a transmembrane protein that is ubiquitously expressed in non-invasive epithelial and tumor cells prior to their epithelialmesenchymal transition (EMT) [13]; however, we have previously shown that E-cad expression also results in hyperproliferation of breast cancer cells, including MDA-MB-231, by promoting activation of the ERK cascade in a similar 3D organoid [4]. Accordingly, proliferation in our spheroid system was measured using the PrestoBlue viability assay and represents the net proliferation of the spheroid that accounts for cell proliferation, cell death, and nutrient access. Net proliferation increased more than four-fold in E-cad+ spheroids compared to E-cad- for the highly proliferative case of 1 mg/mL collagen (Fig. 1C). This enhanced E-caddependent net proliferation was maintained at all collagen concentrations (Supplementary Figure 1A).

By increasing the collagen concentration in the ECM, net proliferation was decreased (Fig. 1D). Specifically, E-cad+ spheroid proliferation was reduced by more than three-fold in 4 mg/mL collagen compared to the 1 mg/mL condition by day 7 of spheroid culture. Less dense matrices sustained higher net proliferation rates over time (Supplementary Figure 1A). Changing the collagen concentration affects several ECM properties including the elastic modulus, pore size, fiber alignment, and cell speed [19]. These proliferation results may be explained by one or more of these ECM properties, which we explore later with the help of a physical model.

As cells invade the collagen bulk, the local cell density is dispersed across the invaded area to facilitate additional cell

proliferation. By immunofluorescence, we confirmed uniform expression of E-cad throughout E-cad+ spheroids, and no expression of E-cad in E-cad- spheroids (Fig. 1E, Supplementary Figure 2A). Proliferation marker Ki-67 was also homogeneously expressed throughout all spheroids, although apoptosis marker Cleaved caspase-3 was elevated in the central region of some conditions (Fig. 1F, Supplementary Figure 2B). Therefore, net spheroid proliferation must be analyzed simultaneously with spheroid invasion to understand the spatial constraints on spheroid growth.

3.1.2. Continuum invasion is promoted by E-cad and limited by collagen

Another key feature of tumor growth is invasion into the surrounding stroma. Invasion dictates the fate of the tumor through spatial expansion, and intrinsically promotes tumor proliferation by dispersing the cell population. We explain this coupling of net spheroid proliferation and continuum invasion through a maximum carrying capacity which we define as the maximum cell count that can be supported by the spheroid volume, nutrient access, and mechanical properties.

When evaluating invasion, it is important to distinguish between continuum and detached phenotypes (Fig. 1B). Our analysis focused on expansion of the spheroid aggregate through continuum invasion where net proliferation and invasion are intrinsically coupled. Intercellular adhesion, which is enhanced by E-cad expression (Fig. 2A), causes an orchestrated response where mechanical waves travel within the spheroid. Propulsion forces from the spheroid's leading edge as peripheral cells invade the collagen bulk and compressive forces from the inner volume as spheroid proliferation increases the cell density within the spheroid are transmitted to the intermediate regions [54]. However, under low intercellular adhesion (E-cad-) such mechanical waves are not transmitted throughout the spheroid, and cells at the outer (leading) surface of the spheroid invade as single cells (detached). To better differentiate these two invasion phenotypes, we defined a continuum region and a detached cell region within our spheroids (Fig. 2B). We determined the extent and phenotype of invasion for each condition by annotating the boundary of the continuum and detached cell regions (Fig. 2C, Supplementary Figure 3). E-cad+ continuum invasion into the collagen bulk was significantly greater than continuum invasion of E-cad- spheroids by day 5 (Fig. 2D, Supplementary Figure 1B).

The cells at the spheroid's leading surface also exert traction forces by reorganizing and pulling on the surrounding collagen fibers as they invade [17]. E-cad regulates this force by forming intercellular adherens junctions [52,53]. In E-cad+ spheroids these interactions facilitate the transmission of cell-ECM traction forces to the dense internal region of the spheroid according to the mechanical waves described above. However, if intercellular adhesion is low, as in E-cad- conditions, the cell-ECM propulsion forces can be strong enough to propel individual peripheral cells outward from the spheroid. High propulsion forces under low adhesion result in cell detachment from the continuum, and, as a consequence, the traction force is not propagated throughout the spheroid continuum. Detached cell invasion was quantified for each spheroid by measuring the average radial distance between the edge of the continuum and the leading invasive front (Fig. 2C). We observed a population of detached cells invading as single cells and others that were travelling as cohesive units in contact with other cells that also detached from the spheroid continuum. The percentage of detached cells traveling as cohesive units or single cells that were elongated was not significantly changed when increasing the collagen concentration (Supplementary Figure 4A). However, single cell units were more common in E-cad- spheroids (Supplementary Figure 4B). Considering all cell populations, detached cells invaded a larger radial distance from the continuum

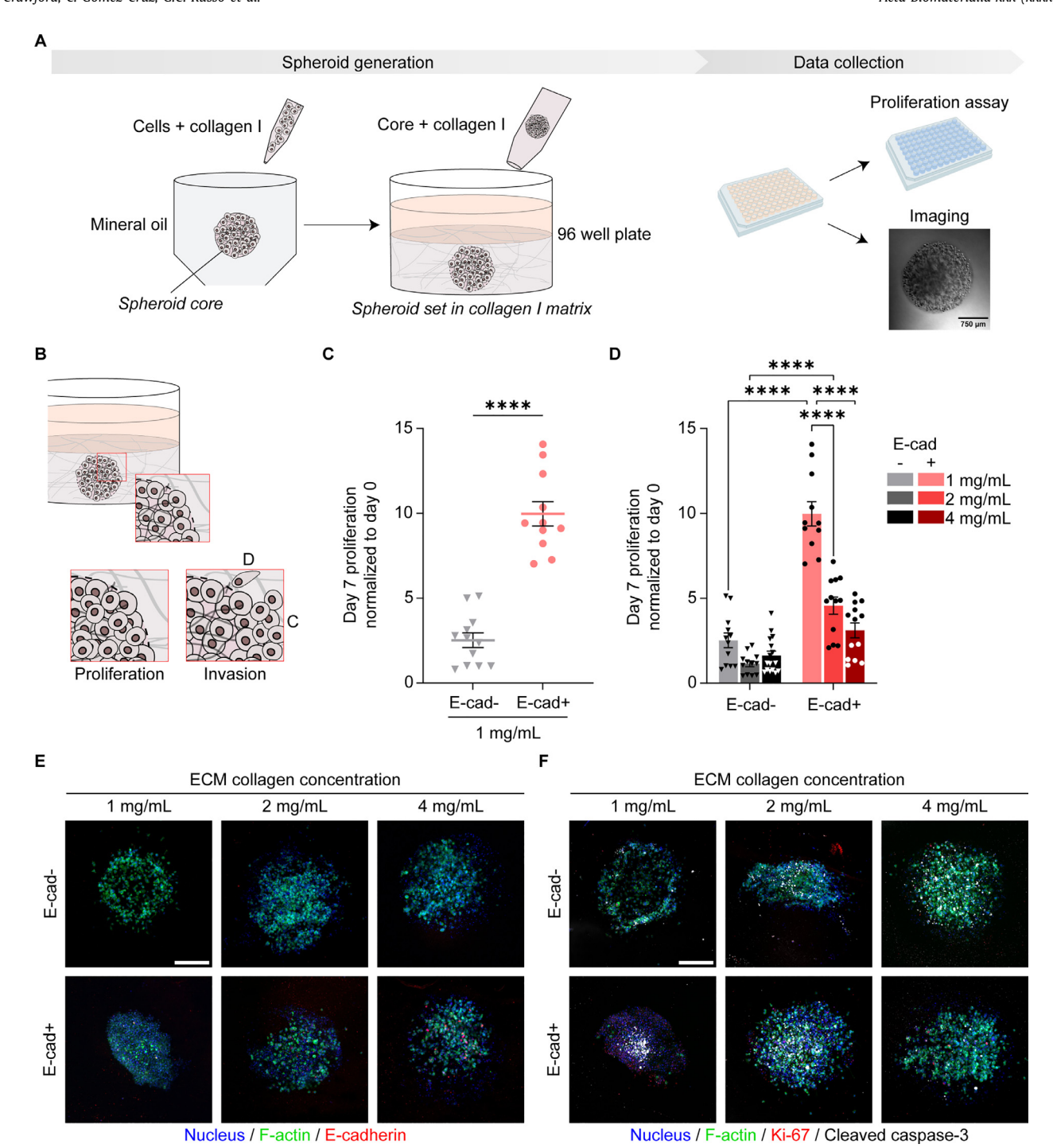


Fig. 1. E-cad expression and ECM composition regulate net proliferation in spheroids. (A) Spheroid generation and data collection schematic. (B) Theoretical representation of spheroid proliferation and invasion. D denotes detached cell invasion, and C denotes continuum invasion. (C) PrestoBlue relative proliferation on day 7 of MDA-MB-231 E-cad-/+ spheroids at 1 mg/mL ECM collagen concentration. Statistical test used: unpaired t-test, ***** $P \le 0.0001$. (D) PrestoBlue relative proliferation of MDA-MB-231 E-cad-/+ spheroids at 1, 2 and 4 mg/mL ECM collagen concentration comparing spheroids on day of generation (day 0) to day 7. Statistical test used: two-way ANOVA with multiple comparisons, **** $P \le 0.0001$. (C) and (D) All data are mean ± SEM for N = 3 biological replicates with n = 3+ technical replicates. (E) Immunofluorescence staining for E-cad-/+ spheroids at all collagen concentrations. (F) Immunofluorescence staining for Ki-67 (red) and Cleaved caspase-3 (gray) in E-cad-/+ spheroids at all collagen concentrations. (E) and (F) Representative images are shown for day 5 spheroids. Images are maximum intensity projections of stacks of confocal microscopy images where the nucleus is stained in blue and F-actin is stained in green. Scale bar, 300 μm.

in E-cad- spheroids than E-cad+ spheroids in the same collagen concentration (Fig. 2E).

Many physical properties of the ECM are impacted by changes to collagen density. For example, an increase in collagen concentration results in a smaller pore size and a change in the elastic modulus of the collagen gel, which limits the ability of cells to reorganize the matrix [19]. As a result, we observed de-

creases in the spheroid continuum area at high collagen concentrations where the elastic modulus is high and the average pore size is low (Fig. 2F, Supplementary Figure 1B). In these conditions, high cell-ECM friction limited spheroid invasion despite the previously described tensile stresses due to E-cad expression. In extreme cases (6 mg/mL collagen), null spheroid expansion was observed.

Acta Biomaterialia xxx (xxxx) xxx

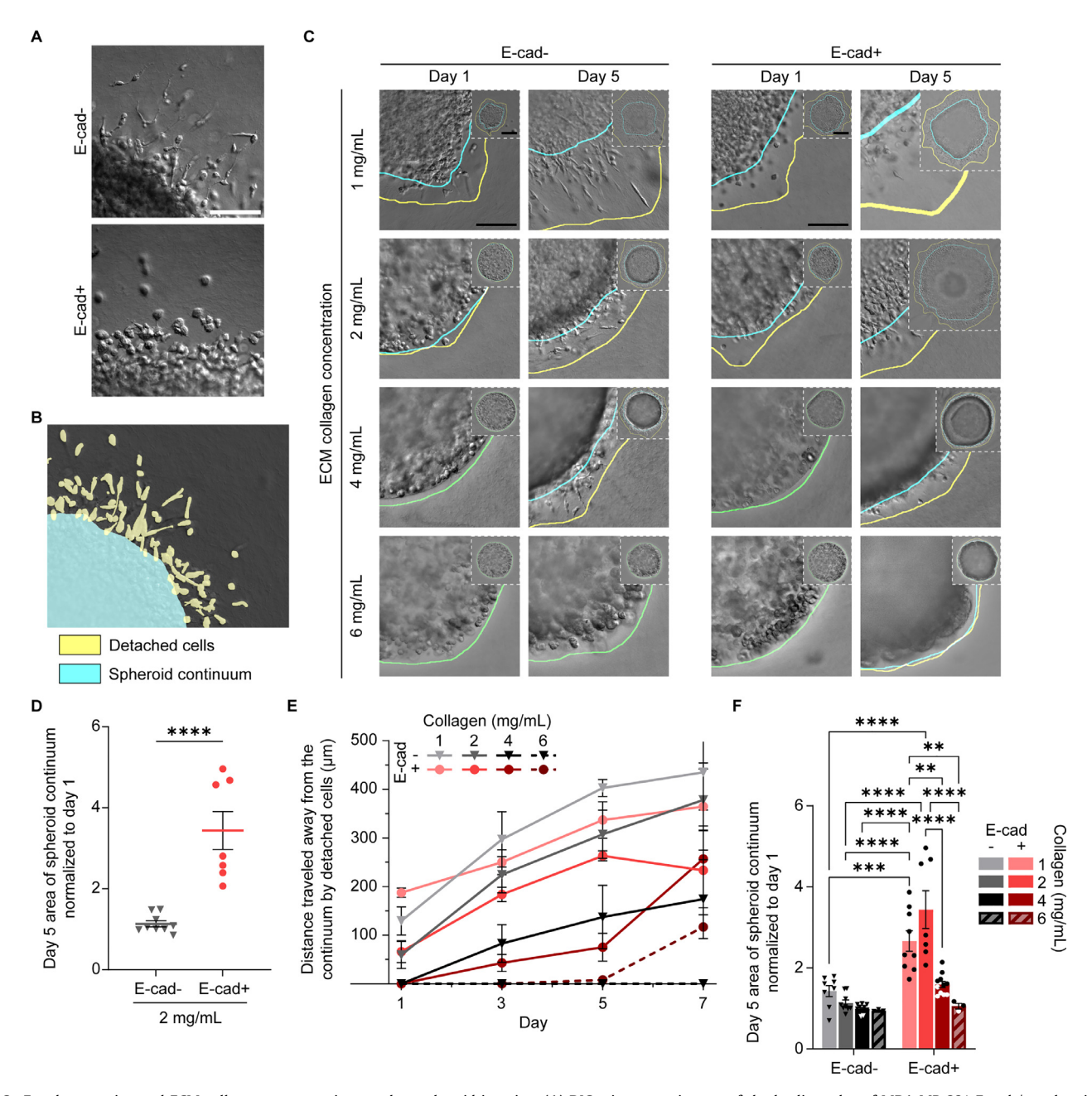


Fig. 2. E-cad expression and ECM collagen concentration regulate spheroid invasion. (A) DIC microscopy images of the leading edge of MDA-MB-231 E-cad-/+ spheroids on day 5. Representative images are shown for 2 mg/mL collagen. Scale bar: 250 μ m. (B) Schematic defining the detached cells region in yellow and the spheroid continuum in cyan. (C) DIC microscopy images of MDA-MB-231 breast cancer cells (E-cad- lentiviral control, left panel) and MDA-MB-231 cells with E-cad lentiviral knock-in (E-cad+, right panel) on day 1 and day 5. Yellow annotations label the detached cells region and cyan annotations label the spheroid continuum. Scale bar: 200 μ m, inset: 500 μ m. (D) E-cad dependent expansion of the spheroid continuum area from day 1 to day 5 in a 2 mg/mL collagen ECM. Statistical test used: unpaired t-test, **** $P \le 0.0001$. (E) Average radial invasion distance of detached cells from the spheroid continuum over time for all E-cad conditions (E-cad-/+) and ECM collagen concentrations (1, 2, 4, 6 mg/mL). The error bar for 1 mg/mL E-cad- on day 7 is cut off to improve visualization of all data. (F) Expansion of the spheroid continuum area from day 1 to day 5 in E-cad- and E-cad+ spheroids at 1, 2, 4 and 6 mg/mL ECM collagen concentration. Statistical test used: two-way ANOVA with multiple comparisons, **** $P \le 0.0001$, *** $P \le 0.001$. The data in (D), (E) and (F) are reported for N = 3 with N = 2-4 for 1, 2 and 4 mg/mL collagen concentrations. The data for 6 mg/mL are included as a limiting case with N = 1 and N = 3. All data are mean N = 3 with N = 3 and N = 3 with N = 3 and N = 3 with N = 3 and N = 3. All data are mean N = 3 with N = 3 with N = 3 and N = 3 with N = 3 with N = 3 and N = 3 with N = 3 with N = 3 and N = 3 with N = 3

It is important to note that the increase in collagen concentration from 1 mg/mL to 2 mg/mL enhanced continuum invasion, while in most other cases, increasing collagen concentration caused a decrease in continuum invasion (Fig. 2E, Supplementary Figure 1B). One explanation is the average pore size of a collagen gel decreases with increasing collagen concentration; however, the elastic modulus of the gel also decreases from 1 to 2 mg/mL [19]. Cells can more easily remodel a gel with a lower elastic modulus to expand the continuum. The increase in collagen fibers could also increase the number of cell-ECM ad-

hesions, thus strengthening the traction force from cells using these adhesions to invade the matrix. We next evaluated this hypothesis by quantifying peripheral cell elongation, which correlates with stronger propulsion forces at the spheroid's boundary [17.41.55].

3.1.3. Boundary propulsion forces are limited by E-cad and promoted by collagen

The ability of cells at the leading edge of the spheroid to exert propulsion forces is in part dependent on the elongation of

Acta Biomaterialia xxx (xxxx) xxx

these cells [17,41,55]. Thus, the elongation of cells at the spheroid boundary contributes to spheroid invasion. A circular cell (epithelial) using ECM fibers as support points in a theoretical homogeneous microenvironment generates a system of contractile forces with radial symmetry so that the resultant force at its center of mass is null. This symmetry prevents the required effective propulsion force for the cell to invade the matrix [17]. If the cell is elongated (mesenchymal), radial symmetry is lost, and an effective force is generated along the direction of elongation [40,41]. This force depends on cell elongation and other features such as the formation of focal adhesions and the stiffness or viscous relaxation of the ECM [41,55,56]. The mechanical behavior of the collagen network presents viscoelastic responses leading to stress relaxation [57]. These effects are known to have important roles in individual cell migration [56]; however, the characteristic times of the multi-cellular spheroid continuum problem are much larger than the collagen network relaxation times, so we assume a negligible role of viscoelastic effects in the proposed formulation. These features can be controlled by E-cad expression and collagen concentration in our spheroid system.

To examine how E-cad expression and collagen concentration regulate the ability of cells to generate the propulsion force required for invasion, we quantified the elongation of cells at the spheroid's edge (Fig. 3A, Supplementary Figure 5). E-cad- cells were significantly more elongated than E-cad+ cells as early as day 3 (Fig. 3B-C, Supplementary Figure 1C-D). This inverse relationship of E-cad expression and elongation is explained by the decrease in intercellular adhesion forces when E-cad is not expressed. At the spheroid-ECM boundary, E-cad- cells can elongate and invade as detached cells by overcoming traction stresses from the cell aggregate. This invasive behavior of a single cell is consistent with mesenchymal cells, which are believed to lose E-cad expression during EMT [12,13]. Alternatively, expression of E-cad (E-cad+) promotes cell-cell adhesion resulting in higher mechanical boundary constraints on the spheroid. These E-cad+ cells had lower elongation scores (Fig. 3A-C) and invaded as a continuum into the surrounding matrix (Fig. 2).

In addition to intercellular dependencies, the extracellular conditions (collagen concentration) influenced cell elongation. Cell elongation increased with increasing collagen concentration; although, the impact of collagen concentration on cell elongation was evident at earlier time points in E-cad- spheroids where an effect could be observed by day 3 (Fig. 3D), but was not observed in E-cad+ spheroids until day 5 (Supplementary Figure 1C-D). The elongated/mesenchymal phenotype is a result of the mechanical balance between traction forces from the spheroid and its surrounding ECM. Therefore, ECM mechanical properties such as elastic modulus and pore size impact cell elongation and spheroid invasion phenotypes by directing the resulting propulsion force and its magnitude. Thus, increasing collagen concentration decreases ECM pore size, but increases the elastic modulus of the gel and the spatial density of collagen fibers that serve as support points for forces exerted by the cells [19]. Cells must adopt more narrow, elongated shapes to navigate a high density

The elongation data presented here with the spheroid proliferation and continuum invasion data presented above demonstrate the coupling of net proliferation and continuum invasion. However, these quantitative experimental observations were limited to net proliferation and invasion measurements that cumulatively account for the system properties we modulated through E-cad expression and ECM collagen concentration, so we turned to a mechanistically-based theoretical model to isolate the individual impacts of each physical property of the system.

3.2. A mechanistically-based theoretical model explains the connection between spheroid proliferation and continuum invasion

3.2.1. Model calibration and validation

Our experimental data demonstrated the importance of both intercellular (E-cad) and extracellular (collagen) mechanical conditions on spheroid proliferation and invasion. The data also showed that these processes are intrinsically linked. E-cad expression promoted net proliferation and hindered cell elongation at the leading edge of the spheroid. An increase in ECM collagen concentration reduced net proliferation and continuum invasion. However, experimental analysis was limited to correlations and did not provide a deeper identification of the specific mechanobiological properties governing such processes. Continuum invasion cannot be delineated from net proliferation through experimental methods.

We developed a physical model formulated at the continuum scale to identify the underlying mechanistic features governing net proliferation and continuum invasion. The biomechanical parameters integrated into the model are illustrated in Fig. 4A. By modulating E-cad expression and collagen concentration in our spheroid experiments, we introduced a combination of biomechanical consequences. The theoretical model serves as a virtual framework to evaluate the independent role of these biomechanical parameters in net spheroid proliferation and continuum invasion.

We first calibrated the model to a reference E-cad+ spheroid with a 4 mg/mL collagen matrix. The large frictional terms in this condition limited continuum invasion, thus we could determine the limiting cell density (ρ_{∞}) of the system. Note that this parameter is fixed for all E-cad and collagen conditions. Further motivation and values for the model parameters are provided in the Methods. Model predictions agreed with experimental data for both continuum invasion (Fig. 4B) and net spheroid proliferation (Fig. 4C). We then tested the model by varying E-cad expression and collagen concentration according to our experimental modulations without further calibration (see Methods). Overall, the model predictions agreed with experimental data (Supplementary Figure 6A-B). Expression of E-cad caused net spheroid proliferation (Fig. 4D) and continuum invasion (Fig. 4E) to increase. Alternatively, increasing collagen concentration decreased spheroid proliferation (Fig. 4F, Supplementary Figure 1E) and continuum invasion (Fig. 4G, Supplementary Figure 1F). The model also predicted limited continuum invasion in the 1 mg/mL collagen conditions (Fig. 4G, Supplementary Figure 1F), matching our experimental data (Fig. 2F, Supplementary Figure 1B).

The model predictions deviated the most from experimental results at late time points for the 1 and 2 mg/mL collagen conditions when E-cad was expressed (Supplementary Figure 6C-D). As previously established, many physical properties of a collagen gel (i.e., pore size, elastic modulus, and fiber alignment) are nonlinearly correlated with collagen concentration [19]. For example, the average pore size of a 1 mg/mL collagen gel is larger than the pore size of 2 mg/mL and 4 mg/mL gels, but the elastic modulus of a 2 mg/mL gel is lower than 1 mg/mL and 4 mg/mL gels. In our model, spheroid-ECM friction refers to the interactive force that opposes spheroid invasion, and spheroid-ECM adhesion refers to interactions with the ECM that produce propulsion forces so the spheroid can invade the matrix. The physical properties of the collagen gel were built into these spheroid-ECM friction and spheroid-ECM adhesion parameters, so some nuances in physical properties were diluted in the model predictions. However, these model predictions maintained the trends observed in our experimental data (increased net proliferation at lower collagen density and continuum invasion peaked at intermediate collagen densities) (Supplementary Figure 1A-B,E-F). Model predictions for all other collagen

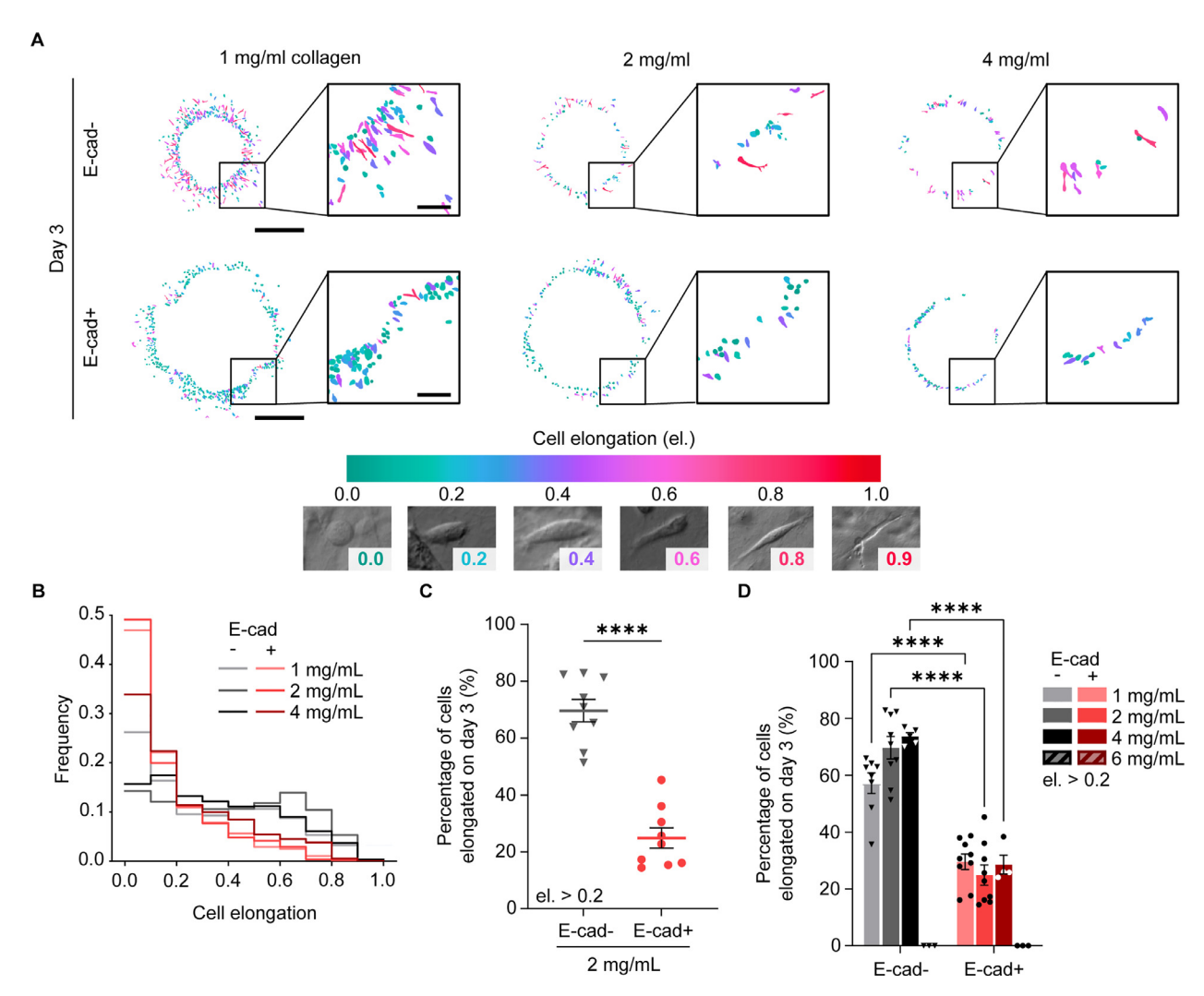


Fig. 3. E-cad expression and ECM concentration regulate cell elongation. (A) Morphology masks of cells detached from spheroids on day 3, where cell elongation was quantified and correlated to the mask color. Examples of cells with elongation 0.0, 0.2, 0.4, 0.6, 0.8 and 0.9 are shown. Scale bar: 1 mm, inset: 250 μm. (B) Relative frequency of cell elongation scores. Cumulative values calculated over days 1, 3, 5 and 7 are shown. (C) Percentage of elongated cells (el. > 0.2) within the detached region by E-cad expression. Data shown are from day 3 at 2 mg/mL collagen. Data are mean ± SEM. Statistical test used: unpaired *t*-test, ***** $P \le 0.0001$. (D) Percentage of cells with el. > 0.2 on day 3 by ECM collagen concentration. Data are mean ± SEM. Statistical test used: two-way ANOVA with multiple comparisons, **** $P \le 0.0001$, ** $P \le$

concentrations and time points were within the distributions of experimental data (Supplementary Figure 6A-B).

3.2.2. Parametric analysis of the continuum model

To better understand the high net proliferation, low continuum invasion, and discrepancies observed between experimental results and model predictions at low collagen concentrations, we studied the influence of each biomechanical parameter (spheroid/cell aggregate stiffness, net spheroid proliferation rate, effective propulsion force, and spheroid-ECM friction, all illustrated in Fig. 4A) using the continuum model.

The effective propulsion force of the spheroid results from cell interactions with collagen fibers. In our parametric analysis, net proliferation and continuum invasion predictions are reported as relative total cell counts and relative continuum radii, respectively. The model predicted that increasing propulsion force caused total cell count and continuum radius to increase (Fig. 5A). The opposite effect was observed when increasing spheroid-ECM friction, which decreased the total cell count and continuum radius (Fig. 5B). The magnitude of these impacts on continuum invasion was greater than the magnitude of the impacts on net spheroid

proliferation. These biomechanical parameters (propulsion force and spheroid-ECM friction) involve extracellular interactions between the spheroid and the ECM; therefore, the bias of these predictions toward continuum invasion was expected.

We consider net spheroid proliferation an intercellular condition due to the dependence on E-cad expression and hyperproliferation via the ERK cascade when activated by cell-cell adherens junctions [4]. Therefore, to predict the impact of intercellular conditions, we altered the stiffness of the cell aggregate and the spheroid proliferation rate, which were simultaneously modulated experimentally through E-cad expression. When adjusting spheroid stiffness only, the model predicted minimal changes to total cell count and continuum radius (Supplementary Figure 7). This prediction suggested that intercellular adhesion has a limited influence on continuum radius and net spheroid proliferation. However, our experimental data revealed a consistent inverse relationship between collagen density and net spheroid proliferation (Fig. 1D, Supplementary Figure 1A), so we theoretically modulated the net proliferation rate under conditions of high and low spheroid-ECM friction (Fig. 5C). Under high friction, the model predicted a moderate increase in total cell count and null change in continuum in-

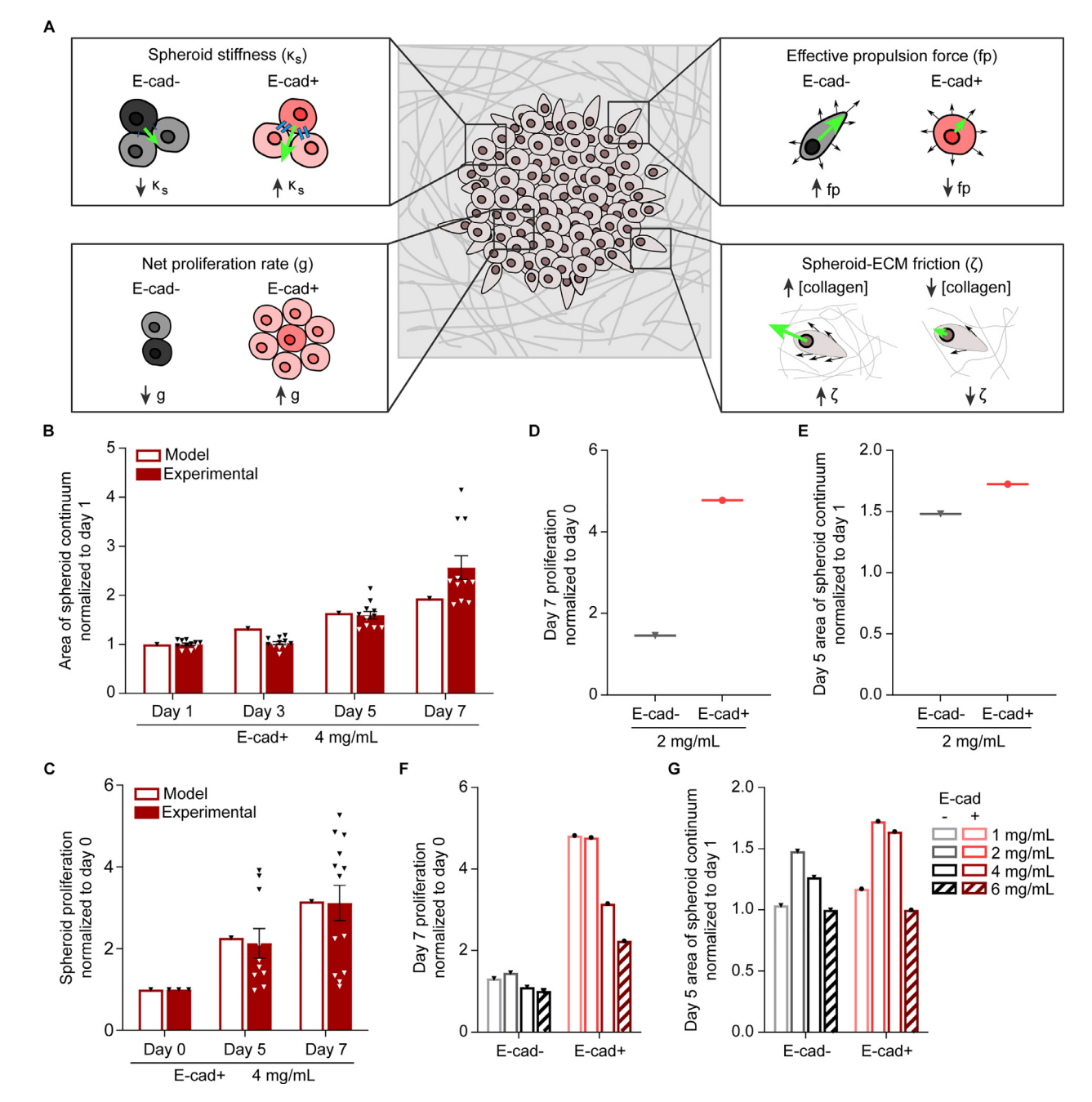


Fig. 4. Spheroid mechanobiology from a continuum modeling perspective. (A) Conceptual basis of the theoretical model representing a continuum spheroid embedded in a collagen matrix. The model accounts for four main biomechanical parameters, which are illustrated: the spheroid cell aggregate stiffness ($κ_s$, top left), the net spheroid proliferation rate (g, bottom left), the effective propulsion force (fp, top right), and spheroid-ECM friction (ζ, bottom right). These parameters are experimentally modulated by changes to cell-cell adhesion, cell proliferation, cell-ECM adhesion, and cell-ECM friction, respectively, which are all influenced by E-cad expression and ECM collagen concentration. Green arrows indicate the direction and magnitude of each force. Model predictions for the reference case (E-cad+, 4 mg/mL collagen) are compared to experimental data: (B) continuum invasion and (C) net spheroid proliferation. Model predictions are outlined and experimental data are solid fill. Experimental data presented in (B) and (C) are mean ± SEM. N = 3, n = 3+. Model predictions based on E-cad expression are presented at 2 mg/mL collagen for (D) net spheroid proliferation and (E) continuum invasion. Model predictions for the influence of ECM collagen concentration on (F) net spheroid proliferation and (G) continuum invasion.

vasion when net proliferation rate was increased. This suggested an important regulatory effect of cell-matrix friction on tumor growth. In conditions where cell-matrix friction inhibited spatial expansion, the maximum carrying capacity of the spheroid system was quickly reached and proliferation was restricted. Under conditions of low cell-ECM friction, the maximum carrying capacity was more fluid because the physical restrictions on the system were reduced. Increasing the net proliferation rate resulted in more significant changes to both cell count and continuum radius when cell-ECM friction was low. This parametric analysis agreed with our ex-

perimental observations and provided additional insight into the influence of individual biomechanical parameters that could not be determined experimentally, specifically, the limiting impact that friction can have on spheroid growth.

3.2.3. Parametric analysis under heterogeneous proliferation rates

Our initial parametric analysis considered a constant proliferation rate throughout all regions of the spheroids. However, our immunofluorescence data (Fig. 1F, Supplementary Figure 2B) demonstrated that the local net proliferation rate can change with radial

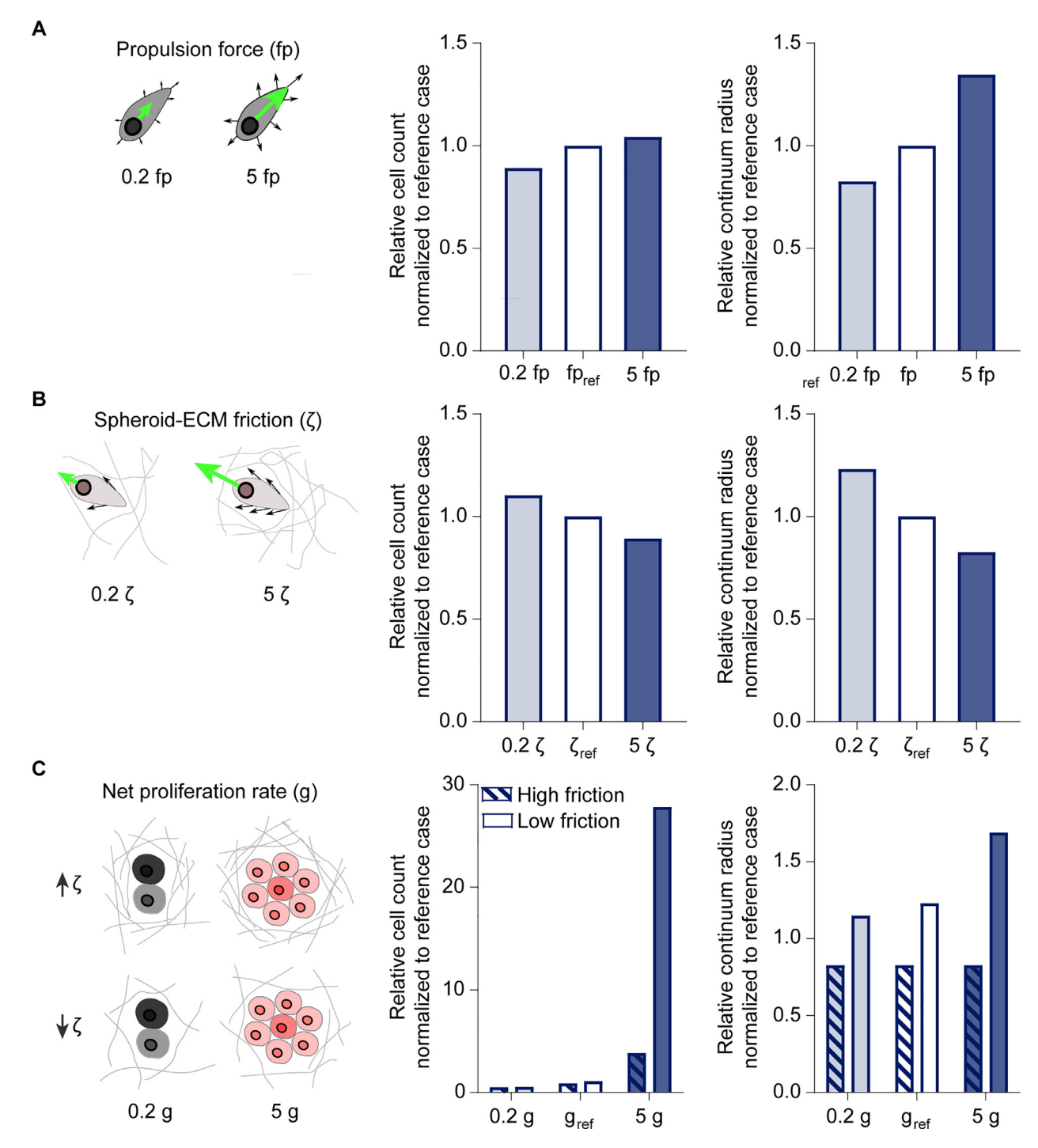


Fig. 5. Parametric analysis of the continuum model. Model predictions of spheroid cell count and continuum radius when modulating the magnitude of extracellular conditions: (A) propulsion force or (B) spheroid-ECM friction. (C) Model predictions of spheroid cell count and continuum radius when modulating the magnitude of net spheroid proliferation rate under high $(5^*\zeta_{ref})$ and low $(0.2^*\zeta_{ref})$ spheroid-ECM friction. Green arrows in the cartoons indicate the direction and magnitude of each force. All results shown were normalized to the reference case used in the simulations: E-cad+ in 4 mg/mL collagen matrix. All mechanical parameters were modified by dividing and multiplying the reference values by 5.

distance from the spheroid core, with more cell death occurring close to the center of the spheroid in most cases. Thus, we adjusted our parametric analysis for propulsion force and spheroid-ECM friction to consider net proliferation rates that increase linearly and exponentially with radial distance from the spheroid core (Fig. 6A). All conditions were calibrated to reach the same spheroid cell count and continuum invasion distances at the end of the simulations (Fig. 6B).

Modulating the spatial distribution of net proliferation rate did not significantly change continuum invasion results; although, the patterns in relative cell counts were more complex (Fig. 6C-D). Under high propulsion forces or low friction, the invasion rate surpasses the proliferation rate. With a heterogeneous distribution of net proliferation, the resulting cell distribution will be a balance between invasion velocity and cell diffusion towards the spheroid core. In the most severe case (exponential), the outer region of the

Acta Biomaterialia xxx (xxxx) xxx

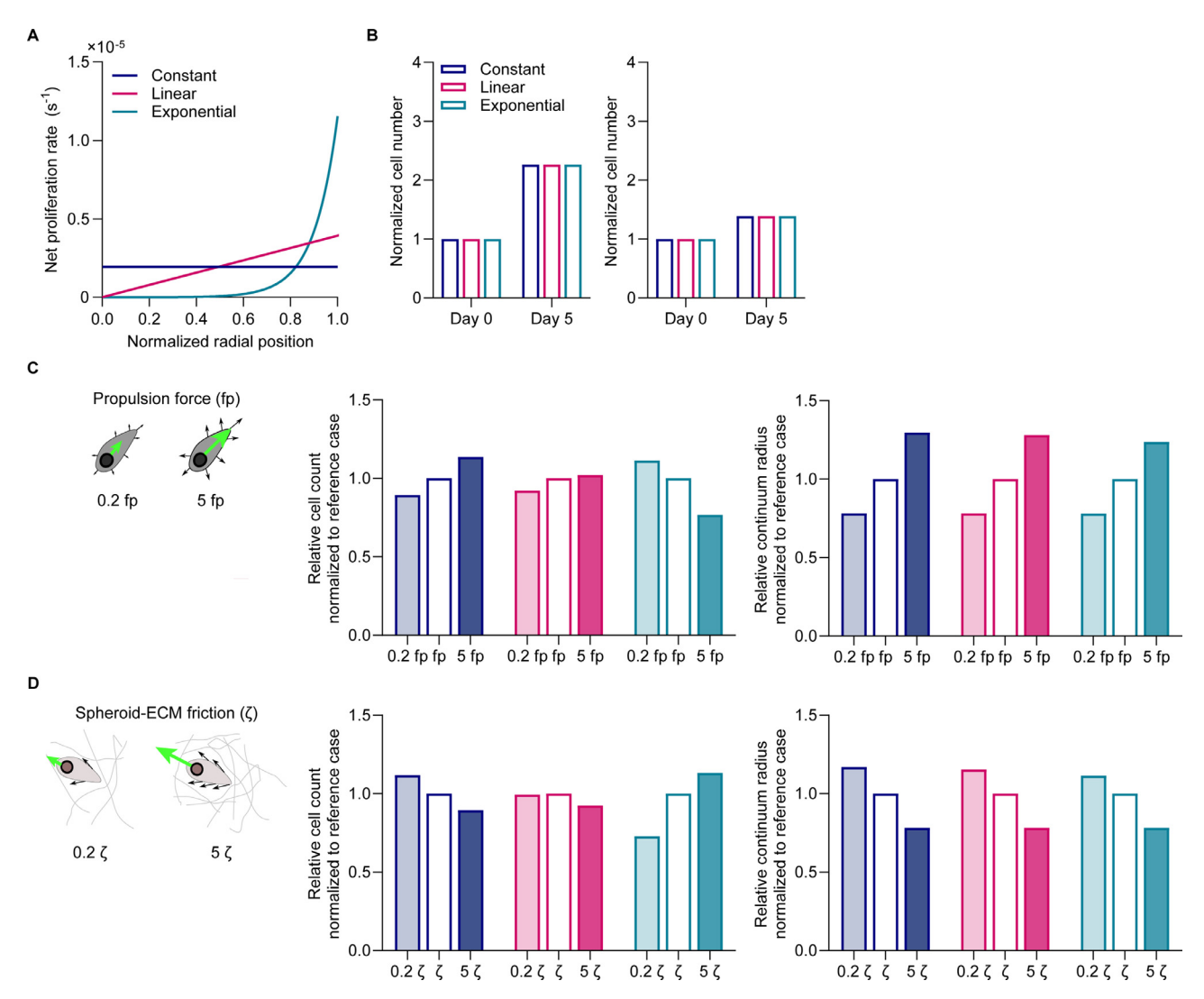


Fig. 6. Parametric analysis of the model with different distributions of proliferating cells. (A) Constant, linear, and exponential distributions of net proliferation rates. (B) Normalized total cell number and continuum radius that result from the different proliferation rate distributions. Model predictions of net spheroid cell count and continuum radius when modulating the magnitude of spheroids biomechanical parameters: (C) propulsion force and (D) spheroid-ECM friction. Green arrows in the cartoons indicate the direction and magnitude of each force. All results shown were normalized to the reference case used in the simulations: E-cad+ in 4 mg/mL collagen matrix. All mechanical parameters were modified by dividing and multiplying the reference values by 5.

spheroid is highly proliferative, but cell diffusion toward the inner core is more difficult as this front invades. The maximum carrying capacity is quickly reached in this region and net spheroid proliferation is limited as a result. Under low propulsion forces and high friction, the spheroid is more confined. When the proliferation rate is exponentially higher at the edges of the spheroid than the center, cells in the highly proliferative outer region can diffuse to less dense areas within the spheroid, reducing spatial saturation and promoting a faster evolution of the system. Here, we consider the effects of a heterogeneous net proliferation rate within the spheroid and demonstrate how this is an important parameter when studying solid tumors where oxygen and nutrient access can cause non-uniform proliferation distributions.

4. Discussion

In this study, we demonstrated the advantages of complementary experimental and computational methodologies when studying tumor mechanobiology. We provided a virtual testbed for the analysis of isolated biomechanical parameters governing net proliferation and continuum invasion of breast cancer tumors based

on experimental data. We modulated the expression of intercellular adhesion protein E-cad and ECM collagen density in our tumor spheroid to observe phenotypic changes in net proliferation and continuum invasion. Each experimental modulation changed an array of physical properties, so we turned to a mechanistically-based theoretical model to understand the isolated effects of each property manipulation on tumor growth.

We first demonstrated that net proliferation and continuum invasion are intrinsically coupled using 3D in vitro assays with breast cancer spheroids. Our data showed that the expression of E-cad enhances net spheroid proliferation and continuum invasion, while increasing the ECM collagen concentration hinders both processes. E-cad expression promotes cell-cell adhesion that limits cell elongation and, a priori, should limit cell invasion [12,13]. However, E-cad expression also increases cell proliferation [4]. The spheroid volume must increase to accommodate the increasing cell count in E-cad+ spheroids, thus the continuum must invade the surrounding stroma. In the experimental model, this invasion due to proliferation cannot be distinguished from invasion due to active cell forces [58–61]. Their relative contributions are explored using the computational model. Increasing the density of collagen, which is

Acta Biomaterialia xxx (xxxx) xxx

secreted in situ by tumor and stromal cells [16–18], changes the pore size and elastic modulus of the matrix [19] leading to higher frictional forces which oppose invasion. If the spheroid cannot volumetrically expand, net proliferation is limited, and vice versa. The tumor spheroid cell count must be sufficient to support continuum invasion into the surrounding matrix. This maximum carrying capacity illustrates the intrinsic coupling of tumor proliferation and continuum invasion.

Experimentally manipulating E-cad expression and collagen concentration causes changes to multiple biomechanical parameters; however, each mechanism's influence on proliferation and invasion cannot be isolated experimentally. So, we developed a continuum model to study the consequences of individually changing biomechanical parameters. For example, our experimental data demonstrated that E-cad expression increases net proliferation (Fig. 1C, Supplementary Figure 1A) and continuum invasion (Fig. 2D, Supplementary Figure 1B), but decreases cell elongation (Fig. 3C, Supplementary Figure 1D). The increase in net proliferation caused compression stresses within the spheroid that were relaxed by expansion of the continuum. However, the increase in cell-cell adhesion and decreased cell elongation, both via E-cad expression, induced a higher mechanical resistance to detached cell invasion (Fig. 2E). Collagen concentration also impacts these spheroid dynamics. When collagen concentration increases, cell-ECM friction and cell elongation increase (Fig. 3D, Supplementary Figure 1D). These results agree with previous studies where cells adapted their polarity to adjust for increased friction in higher concentration collagen gels [62]. The resulting system balance is a competition between propulsion forces, which increase with cell elongation, and increased friction. Experimentally, a maximum carrying capacity with these physical properties could be observed via limited proliferation in high concentration collagen matrices, but experimental quantification of individual cell nuclei by microscopy is challenging due to the opacity of a highly packed spheroid core. The continuum model facilitated predictions of the independent impacts of each biomechanical parameter on net proliferation and continuum invasion to explain that maximum carrying capacity.

The model was calibrated with the E-cad+ 4 mg/mL collagen experimental data because continuum invasion was limited but spheroid proliferation was still observed, thus a limiting cell density could be defined for this condition. After calibration, all parameters that varied between conditions were directly obtained from experimental values either measured for this work or found in the literature. Spheroid stiffness values were obtained from the literature, where cell stiffness can vary [63-66]. Note that the tensile stiffness referenced from previously published literature was reported as the number of E-cad-E-cad bonds between two cells in 2D [67]. For the 3D assumption used here, this value is an approximation [67]. Nevertheless, parametric analysis of spheroid stiffness revealed a small contribution to the overall continuum dynamics compared to the other biomechanical parameters (Fig. 5, Supplementary Figure 7), which minimizes the effect of these reported approximations on the model outcomes.

The model accurately predicted most experimental results with this calibration; however, the prediction error for late time points (day 5 and day 7) in E-cad+ spheroids at 1 and 2 mg/mL collagen concentration was increased (Supplementary Figure 6C,D). This increase in prediction error could be caused by experimental variation, especially on day 7 of the E-cad+ 2 mg/mL condition where continuum invasion varied significantly across biological replicates (Supplementary Figure 6B). Another possible explanation is cell remodeling and degradation of the ECM, which is not considered in the current formulation. This may be important at later stages of the spheroid invasion process, specifically in low collagen concentrations that lead to networks that are softer and easier to remodel. Finally, the nonlinear relationship between collagen concentration

and many of the physical properties of the gel may contribute as well [19]. In particular, elastic modulus and pore size have a significant impact on the ability of cells to invade the matrix. These collagen gel properties were collectively incorporated into the model through parameters such as spheroid-ECM friction, so some of the effects of these physical gel properties were diluted in the net proliferation and continuum invasion predictions.

Another notable observation is the low continuum invasion that was experimentally observed and computationally predicted in 1 mg/mL collagen matrices (Figs. 2F, 4G, Supplementary Figure 1B,F). Despite elevated net proliferation rates at this collagen density (Figs. 1D, 4F, Supplementary Figure 1A,E), continuum invasion was limited. While low collagen density means frictional forces are reduced, cell elongation was lowest in the 1 mg/mL collagen conditions (Fig. 3B,D, Supplementary Figure 1C,D), so the propulsion forces at the leading edge of the spheroid were not sufficient for the continuum to invade the matrix. Detached cell invasion requires smaller propulsion forces, so these elongation effects were not as prevalent in the detached cell invasion results (Fig. 2E).

The theoretical framework is conceptualized from a continuum basis and aims to model net proliferation and invasion as a cell aggregate (continuum) rather than as single cells (detached). We chose this approach to best study the proliferation and invasion of E-cad+ tumors, which report decreased survival compared to E-cad- breast cancers [14,15]. Detached cells (single cells), arising in E-cad- spheroids, should be studied through alternative models (i.e., single-cell invasion models [68-71], mechanistic protrusivebased models [72-74], motor-clutch based models [56,75], or multiscale approaches [76,77]) that could be added onto a later version of our model studying cancer metastasis during tumor growth. Matrix remodeling by cancer cells during tumor progression has not been explored in this work, but can play a critical role in spheroid progression, particularly at later stages. Analyzing collagen synthesis and deposition, as well as the expression of remodeling enzymes such as matrix metalloproteinases would provide additional insights into the physical forces that guide spheroid progression [78,79]. The continuum model could also be expanded to individually incorporate pore size and elastic modulus of the gel, or local nutrient access, which were built into the spheroid-ECM friction and net proliferation rate terms in our current model. The influences of these parameters on the maximum carrying capacity of the system are synonymous with their impact on net spheroid proliferation and continuum invasion, and thus, tumor growth, which we evaluated in this work.

Author contributions

D.G.G. developed the hypothesis with input from G.C.R., D.W., and A.J.C experimentally, and A.M.B. computationally. A.J.C., G.C.R., and D.W. designed experiments. A.J.C. performed most experiments. G.C.R., W.H., I.B., and T.R. assisted with the experiments. C.G.C. performed most image and data analysis with input from D.G.G and A.M.B.. A.J.C. assisted with data analysis. D.G.G. developed and implemented the computational model. C.G.C. assisted with the implementation of the computational model. D.G.G. and A.J.C. wrote the manuscript with input from C.G.C., G.C.R., D.W., and A.M.B.

Data and materials availability

All data are available in the main text or the supplementary materials. Data for select collagen concentrations and timepoints are presented in the main figures for clarity. Data for all conditions are presented in the supplementary material. Computational models, raw data, and cell lines used in this work are available upon request.

Acta Biomaterialia xxx (xxxx) xxx

Declaration of Competing Interest

The authors declare that they have no known competing financial interests or personal relationships that could have appeared to influence the work reported in this paper.

Acknowledgements

Funding: This work was supported through grants from the National Institute of Health (R01CA174388) to D.W., the National Cancer Institute (U54CA143868 and U54CA268083) to D.W., the National Institute of Arthritis and Musculoskeletal and Skin Diseases (U54AR081774) to D. W., and the National Institute on Aging (U01AG060903) to D.W., D.G.G, C.G.C and A.M.B. acknowledge support from the European Research Council (ERC) under the European Union's Horizon 2020 Research and Innovation Program (Grant agreement No. 947723, project: 4D-BIOMAP). The authors also acknowledge support from the Ministerio de Ciencia, Innovacion y' Universidades, Agencia Estatal de Investigacion, under grant PID2019-109820RB-I00, MCIN/AEI/10.13039' /501100011033, cofinanced by European Regional Development Fund (ERDF), "A way of making Europe," to A.M.B.. C.G.C acknowledges support from the Ministerio de Universidades, Spain (FPU20/01459) and A.M.B. from Universidad Carlos III de Madrid ("Ayudas para la recualificacion del profesorado funcionario" o contratado").

Supplementary materials

Supplementary material associated with this article can be found, in the online version, at doi:10.1016/j.actbio.2023.12.043.

References

- [1] D. Hanahan, R.A. Weinberg, The hallmarks of cancer, Cell 100 (2000) 57–70, doi:10.1016/S0092-8674(00)81683-9.
- [2] Y.A. Fouad, C. Aanei, Revisiting the hallmarks of cancer, Am J. Cancer Res. 7 (2017) 1016–1036.
- [3] D. Wirtz, K. Konstantopoulos, P.C. Searson, The physics of cancer: the role of physical interactions and mechanical forces in metastasis, Nat. Rev. Cancer 11 (2011) 512–522, doi:10.1038/nrc3080.
- [4] G.C. Russo, A.J. Crawford, D. Clark, J. Cui, R. Carney, M.N. Karl, B. Su, B. Starich, T.-S. Lih, P. Kamat, Q. Zhang, P.-H. Wu, M.-H. Lee, H.S. Leong, V.W. Rebecca, H. Zhang, D. Wirtz, E-cadherin interacts with EGFR resulting in hyper-activation of ERK in multiple models of breast cancer, Biorxiv (2022).
- [5] V. Padmanaban, I. Krol, Y. Suhail, B.M. Szczerba, N. Aceto, J.S. Bader, A.J. Ewald, E-cadherin is required for metastasis in multiple models of breast cancer, Nature 573 (2019) 439–444, doi:10.1038/s41586-019-1526-3.
- [6] G. Berx, F. Van Roy, The E-cadherin/catenin complex: an important gatekeeper in breast cancer tumorigenesis and malignant progression, Breast Cancer Res. 3 (2001) 289, doi:10.1186/bcr309.
- [7] Y.I. Petrova, L. Schecterson, B.M. Gumbiner, Roles for E-cadherin cell surface regulation in cancer, Mol. Biol. Cell 27 (2016) 3233–3244, doi:10.1091/mbc. E16-01-0058.
- [8] W. Yu, L. Yang, T. Li, Y. Zhang, Cadherin signaling in cancer: its functions and role as a therapeutic target, Front. Oncol. 9 (2019), doi:10.3389/fonc.2019. 00989
- [9] E.A. Rakha, D. Abd El Rehim, S.E. Pinder, S.A. Lewis, I.O. Ellis, E-cadherin expression in invasive non-lobular carcinoma of the breast and its prognostic significance, Histopathology 46 (2005) 685–693, doi:10.1111/j.1365-2559.2005. 02156 x
- [10] T.-Y. Na, L. Schecterson, A.M. Mendonsa, B.M. Gumbiner, The functional activity of E-cadherin controls tumor cell metastasis at multiple steps, Proceed. Nat. Acad. Sci. 117 (2020) 5931–5937, doi:10.1073/pnas.1918167117.
- [11] T. Lecuit, A.S. Yap, E-cadherin junctions as active mechanical integrators in tissue dynamics, Nat. Cell Biol. 17 (2015) 533–539, doi:10.1038/ncb3136.
- [12] J.P. Thiery, H. Acloque, R.Y.J. Huang, M.A. Nieto, Epithelial-Mesenchymal Transitions in Development and Disease, Cell 139 (2009) 871–890, doi:10.1016/j.cell. 2009.11.007.
- [13] K. Polyak, R.A. Weinberg, Transitions between epithelial and mesenchymal states: acquisition of malignant and stem cell traits, Nat. Rev. Cancer 9 (2009) 265–273. doi:10.1038/nrc2620.
- [14] M. Ringnér, E. Fredlund, J. Häkkinen, Å. Borg, J. Staaf, GOBO: gene expression-based outcome for breast cancer online, PLoS One 6 (2011) e17911, doi:10. 1371/journal.pone.0017911.

- [15] K. Chu, K.M. Boley, R. Moraes, S.H. Barsky, F.M. Robertson, The Paradox of E-Cadherin: role in response to hypoxia in the tumor microenvironment and regulation of energy metabolism, Oncotarget 4 (2013) 446–462, doi:10.18632/oncotarget.872.
- [16] I. Acerbi, L. Cassereau, I. Dean, Q. Shi, A. Au, C. Park, Y.Y. Chen, J. Liphardt, E.S. Hwang, V.M. Weaver, Human breast cancer invasion and aggression correlates with ECM stiffening and immune cell infiltration, Integrative Biol. 7 (2015) 1120–1134, doi:10.1039/c5ib00040h.
- [17] A.M. Jimenez Valencia, P.-H. Wu, O.N. Yogurtcu, P. Rao, J. DiGiacomo, I. Godet, L. He, M.-H. Lee, D. Gilkes, S.X. Sun, D. Wirtz, Collective cancer cell invasion induced by coordinated contractile stresses, Oncotarget 6 (2015) 43438–43451, doi:10.18632/oncotarget.5874.
- [18] D.M. Gilkes, G.L. Semenza, D. Wirtz, Hypoxia and the extracellular matrix: drivers of tumour metastasis, Nat. Rev. Cancer 14 (2014) 430–439, doi:10.1038/ nrc3726
- [19] S.I. Fraley, P. Wu, L. He, Y. Feng, R. Krisnamurthy, G.D. Longmore, D. Wirtz, Three-dimensional matrix fiber alignment modulates cell migration and MT1-MMP utility by spatially and temporally directing protrusions, Sci. Rep. 5 (2015) 14580, doi:10.1038/srep14580.
- [20] B. Deng, Z. Zhao, W. Kong, C. Han, X. Shen, C. Zhou, Biological role of matrix stiffness in tumor growth and treatment, J. Transl. Med. 20 (2022) 540, doi:10. 1186/s12967-022-03768-y.
- [21] T. Koorman, K.A. Jansen, A. Khalil, P.D. Haughton, D. Visser, M.A.K. Rätze, W.E. Haakma, G. Sakalauskaitè, P.J. van Diest, J. de Rooij, P.W.B. Derksen, Spatial collagen stiffening promotes collective breast cancer cell invasion by reinforcing extracellular matrix alignment, Oncogene 41 (2022) 2458–2469, doi:10.1038/s41388-022-02258-1.
- [22] P. Lu, K. Takai, V.M. Weaver, Z. Werb, Extracellular matrix degradation and remodeling in development and disease, Cold Spring Harb. Perspect. Biol. 3 (2011), doi:10.1101/cshperspect.a005058.
- [23] E. Kuhl, Growing matter: a review of growth in living systems, J. Mech. Behav. Biomed. Mater. 29 (2014) 529–543, doi:10.1016/j.jmbbm.2013.10.009.
- [24] A. Carrasco-Mantis, T. Randelovic, H. Castro-Abril, I. Ochoa, M. Doblaré, J.A. Sanz-Herrera, A mechanobiological model for tumor spheroid evolution with application to glioblastoma: a continuum multiphysics approach, Comput. Biol. Med. 159 (2023) 106897, doi:10.1016/j.compbiomed.2023.106897.
- [25] M.-H. Lee, G.C. Russo, Y.S. Rahmanto, W. Du, A.J. Crawford, P.-H. Wu, D. Gilkes, A. Kiemen, T. Miyamoto, Y. Yu, M. Habibi, I.-M. Shih, T.-L. Wang, D. Wirtz, Multi-compartment tumor organoids, Materials Today 61 (2022) 104–116, doi:10.1016/j.mattod.2022.07.006.
- [26] M.-H. Lee, P.-H. Wu, J.R. Staunton, R. Ros, G.D. Longmore, D. Wirtz, Mismatch in mechanical and adhesive properties induces pulsating cancer cell migration in epithelial monolayer, Biophys. J. 102 (2012) 2731–2741, doi:10.1016/j.bpj.2012. 05.005
- [27] K.E. Kubow, A.R. Horwitz, Reducing background fluorescence reveals adhesions in 3D matrices, Nat. Cell Biol. 13 (2011) 3–5, doi:10.1038/ncb0111-3.
- [28] S.I. Fraley, Y. Feng, A. Giri, G.D. Longmore, D. Wirtz, Dimensional and temporal controls of three-dimensional cell migration by zyxin and binding partners, Nat. Commun. 3 (2012) 719, doi:10.1038/ncomms1711.
- [29] S.I. Fraley, Y. Feng, R. Krishnamurthy, D.-H. Kim, A. Celedon, G.D. Longmore, D. Wirtz, A distinctive role for focal adhesion proteins in three-dimensional cell motility, Nat. Cell Biol. 12 (2010) 598–604, doi:10.1038/ncb2062.
- [30] J.F. Dekkers, M. Alieva, L.M. Wellens, H.C.R. Ariese, P.R. Jamieson, A.M. Vonk, G.D. Amatngalim, H. Hu, K.C. Oost, H.J.G. Snippert, J.M. Beekman, E.J. Wehrens, J.E. Visvader, H. Clevers, A.C. Rios, High-resolution 3D imaging of fixed and cleared organoids, Nat. Protoc. 14 (2019) 1756–1771, doi:10.1038/s41596-019-0160-8.
- [31] S. Preibisch, S. Saalfeld, P. Tomancak, Globally optimal stitching of tiled 3D microscopic image acquisitions, Bioinformatics 25 (2009) 1463–1465, doi:10. 1093/bioinformatics/btp184.
- [32] W. Rasband, Circularity, (2000). https://imagej.net/ij/plugins/circularity.html (accessed June 14, 2023).
- [33] Y.L. Huang, C. Tung, A. Zheng, B.J. Kim, M. Wu, Interstitial flows promote amoeboid over mesenchymal motility of breast cancer cells revealed by a three dimensional microfluidic model, Integrative Biol. 7 (2015) 1402–1411, doi:10.1039/C5IB00115C.
- [34] M.I. Setyawati, C. Sevencan, B.H. Bay, J. Xie, Y. Zhang, P. Demokritou, D.T. Leong, Nano-TiO2 drives epithelial-mesenchymal transition in intestinal epithelial cancer cells, Small 14 (2018) 1800922, doi:10.1002/smll.201800922.
- [35] B. de Melo Quintela, S. Hervas-Raluy, J.M. Garcia-Aznar, D. Walker, K.Y. Wertheim, M. Viceconti, A theoretical analysis of the scale separation in a model to predict solid tumour growth, J. Theor. Biol. 547 (2022) 111173, doi:10.1016/j.jtbi.2022.111173.
- [36] I. González-Valverde, J.M. García-Aznar, Mechanical modeling of collective cell migration: an agent-based and continuum material approach, Comput. Methods Appl. Mech. Eng. 337 (2018) 246–262, doi:10.1016/j.cma.2018.03.036.
- [37] R. Alert, C. Blanch-Mercader, J. Casademunt, Active Fingering Instability in Tissue Spreading, Phys. Rev. Lett. 122 (2019) 088104, doi:10.1103/PhysRevLett.122.
- [38] S. Banerjee, M.C. Marchetti, Continuum Models of Collective Cell Migration, 2019, pp. 45–66, doi:10.1007/978-3-030-17593-1_4.
- [39] T. Bhattacharjee, D.B. Amchin, R. Alert, J.A. Ott, S.S. Datta, Chemotactic smoothing of collective migration, eLife 11 (2022), doi:10.7554/eLife.71226.
- [40] D. Garcia-Gonzalez, A. Muñoz-Barrutia, Computational insights into the influence of substrate stiffness on collective cell migration, Extreme Mech. Lett. 40 (2020) 100928, doi:10.1016/j.eml.2020.100928.

Acta Biomaterialia xxx (xxxx) xxx

- [41] R. Alert, X. Trepat, Physical Models of Collective Cell Migration, Annu. Rev. Condens. Matter Phys. 11 (2020) 77–101, doi:10.1146/annurev-conmatphys-031218-013516.
- [42] E. Comellas, S. Budday, J.-P. Pelteret, G.A. Holzapfel, P. Steinmann, Modeling the porous and viscous responses of human brain tissue behavior, Comput. Methods Appl. Mech. Eng. 369 (2020) 113128, doi:10.1016/j.cma.2020.113128.
- [43] M.S. Zarzor, S. Kaessmair, P. Steinmann, I. Blümcke, S. Budday, A two-field computational model couples cellular brain development with cortical folding, Brain Multiphys 2 (2021) 100025, doi:10.1016/j.brain.2021.100025.
- [44] E. Comellas, J.E. Farkas, G. Kleinberg, K. Lloyd, T. Mueller, T.J. Duerr, J.J. Muñoz, J.R. Monaghan, S.J. Shefelbine, Local mechanical stimuli correlate with tissue growth in axolotl salamander joint morphogenesis, Proc. R. Soc. B: Biol. Sci. 289 (2022), doi:10.1098/rspb.2022.0621.
- [45] D. Ambrosi, M.Ben Amar, C.J. Cyron, A. DeSimone, A. Goriely, J.D. Humphrey, E. Kuhl, Growth and remodelling of living tissues: perspectives, challenges and opportunities, J. R. Soc. Interface 16 (2019) 20190233, doi:10.1098/rsif.2019. 0233
- [46] S. Budday, P. Steinmann, On the influence of inhomogeneous stiffness and growth on mechanical instabilities in the developing brain, Int. J. Solids Struct. 132–133 (2018) 31–41, doi:10.1016/j.ijsolstr.2017.08.010.
- [47] E.K. Rodriguez, A. Hoger, A.D. McCulloch, Stress-dependent finite growth in soft elastic tissues, J. Biomech. 27 (1994) 455–467, doi:10.1016/0021-9290(94) 90021-3.
- [48] D. Garcia-Gonzalez, C.M. Landis, Magneto-diffusion-viscohyperelasticity for magneto-active hydrogels: rate dependences across time scales, J. Mech. Phys. Solids 139 (2020) 103934, doi:10.1016/j.jmps.2020.103934.
- [49] C. Durcan, M. Hossain, G. Chagnon, D. Perić, L. Bsiesy, G. Karam, E. Girard, Experimental investigations of the human oesophagus: anisotropic properties of the embalmed muscular layer under large deformation, Biomech. Model. Mechanobiol. 21 (2022) 1169–1186, doi:10.1007/s10237-022-01583-4.
- [50] D. Faghihi, X. Feng, E.A.B.F. Lima, J.T. Oden, T.E. Yankeelov, A coupled mass transport and deformation theory of multi-constituent tumor growth, J. Mech. Phys. Solids 139 (2020) 103936, doi:10.1016/j.jmps.2020.103936.
- [51] V.A. Lubarda, A. Hoger, On the mechanics of solids with a growing mass, Int. J. Solids Struct. 39 (2002) 4627–4664, doi:10.1016/S0020-7683(02)00352-9.
- [52] A. Stockinger, A. Eger, J. Wolf, H. Beug, R. Foisner, E-cadherin regulates cell growth by modulating proliferation-dependent β-catenin transcriptional activity, J. Cell Biol. 154 (2001) 1185–1196, doi:10.1083/jcb.200104036.
- [53] C. Soler, C. Grangeasse, L.G. Baggetto, O. Damour, Dermal fibroblast proliferation is improved by β-catenin overexpression and inhibited by E-cadherin expression, FEBS Lett. 442 (1999) 178–182, doi:10.1016/S0014-5793(98)01648-2.
- [54] N. Hino, L. Rossetti, A. Marín-Llauradó, K. Aoki, X. Trepat, M. Matsuda, T. Hirashima, ERK-mediated mechanochemical waves direct collective cell polarization, Dev. Cell 53 (2020) 646–660.e8, doi:10.1016/j.devcel.2020.05.011.
- [55] F. Merino-Casallo, M.J. Gomez-Benito, S. Hervas-Raluy, J.M. Garcia-Aznar, Unravelling cell migration: defining movement from the cell surface, Cell Adh. Migr. 16 (2022) 25–64, doi:10.1080/19336918.2022.2055520.
- [56] K. Adebowale, Z. Gong, J.C. Hou, K.M. Wisdom, D. Garbett, H. Lee, S. Nam, T. Meyer, D.J. Odde, V.B. Shenoy, O. Chaudhuri, Enhanced substrate stress relaxation promotes filopodia-mediated cell migration, Nat. Mater. 20 (2021) 1290–1299, doi:10.1038/s41563-021-00981-w.
- [57] D. Tsvirkun, J. Revilloud, A. Giannetti, C. Verdier, The intriguing role of collagen on the rheology of cancer cell spheroids, J. Biomech. 141 (2022) 111229, doi:10. 1016/j.jbiomech.2022.111229.
- [58] Y. Zhang, F. Jiang, Y.C. Zhao, A.-N. Cho, G. Fang, C.D. Cox, H. Zreiqat, Z.F. Lu, H. Lu, L.A. Ju, 3D spheroid-microvasculature-on-a-chip for tumor-endothelium mechanobiology interplay, Biomed. Mater. 18 (2023) 055008, doi:10.1088/ 1748-605X/ace734
- [59] L. Guillaume, L. Rigal, J. Fehrenbach, C. Severac, B. Ducommun, V. Lobjois, Characterization of the physical properties of tumor-derived spheroids reveals critical insights for pre-clinical studies, Sci. Rep. 9 (2019) 6597, doi:10.1038/ s41598-019-43090-0.
- [60] A.V. Taubenberger, S. Girardo, N. Träber, E. Fischer-Friedrich, M. Kräter, K. Wagner, T. Kurth, I. Richter, B. Haller, M. Binner, D. Hahn, U. Freudenberg, C. Werner, J. Guck, 3D microenvironment stiffness regulates tumor spheroid growth and mechanics via p21 and ROCK, Adv. Biosyst. 3 (2019), doi:10.1002/adbi.201900128.

- [61] T. Hasebe, S. Sasaki, S. Imoto, A. Ochiai, Highly proliferative fibroblasts forming fibrotic focus govern metastasis of invasive ductal carcinoma of the breast, Modern Pathol. 14 (2001) 325–337, doi:10.1038/modpathol.3880310.
- [62] M. Cóndor, C. Mark, R.C. Gerum, N.C. Grummel, A. Bauer, J.M. García-Aznar, B. Fabry, Breast cancer cells adapt contractile forces to overcome steric hindrance, Biophys. J. 116 (2019) 1305–1312, doi:10.1016/j.bpj.2019.02.029.
- [63] M. Nikkhah, J.S. Strobl, E.M. Schmelz, M. Agah, Evaluation of the influence of growth medium composition on cell elasticity, J. Biomech. 44 (2011) 762–766, doi:10.1016/j.ibiomech.2010.11.002.
- [64] K. Pogoda, J. Jaczewska, J. Wiltowska-Zuber, O. Klymenko, K. Zuber, M. Fornal, M. Lekka, Depth-sensing analysis of cytoskeleton organization based on AFM data, Eur. Biophys. J. 41 (2012) 79–87, doi:10.1007/s00249-011-0761-9.
- [65] K. Hayashi, M. Iwata, Stiffness of cancer cells measured with an AFM indentation method, J. Mech. Behav. Biomed. Mater. 49 (2015) 105–111, doi:10.1016/j. imbhm 2015 04 030
- [66] C. Voutouri, T. Stylianopoulos, Accumulation of mechanical forces in tumors is related to hyaluronan content and tissue stiffness, PLoS One 13 (2018) e0193801, doi:10.1371/journal.pone.0193801.
- [67] S. Bajpai, J. Correia, Y. Feng, J. Figueiredo, S.X. Sun, G.D. Longmore, G. Suriano, D. Wirtz, α-Catenin mediates initial E-cadherin-dependent cell-cell recognition and subsequent bond strengthening, Proc. Nat. Acad. Sci. 105 (2008) 18331–18336, doi:10.1073/pnas.0806783105.
- [68] E.J. Campbell, P. Bagchi, A computational study of amoeboid motility in 3D: the role of extracellular matrix geometry, cell deformability, and cellmatrix adhesion, Biomech. Model. Mechanobiol. 20 (2021) 167–191, doi:10. 1007/s10237-020-01376-7.
- [69] A. Ippolito, V.S. Deshpande, Contact guidance via heterogeneity of substrate elasticity, Acta Biomater. 163 (2023) 158–169, doi:10.1016/j.actbio.2021. 11.024.
- [70] A. Ippolito, A. DeSimone, V.S. Deshpande, Contact guidance as a consequence of coupled morphological evolution and motility of adherent cells, Biomech. Model. Mechanobiol. 21 (2022) 1043–1065, doi:10.1007/s10237-022-01570-9.
- [71] M.-C. Kim, Y.R. Silberberg, R. Abeyaratne, R.D. Kamm, H.H. Asada, Computational modeling of three-dimensional ECM-rigidity sensing to guide directed cell migration, Proc. Nat. Acad. Sci. 115 (2018), doi:10.1073/pnas.1717230115.
- [72] B.M. Yeoman, P. Katira, A stochastic algorithm for accurately predicting path persistence of cells migrating in 3D matrix environments, PLoS One 13 (2018) e0207216, doi:10.1371/journal.pone.0207216.
- [73] F. Merino-Casallo, M.J. Gomez-Benito, R. Martinez-Cantin, J.M. Garcia-Aznar, A mechanistic protrusive-based model for 3D cell migration, Eur. J. Cell Biol. 101 (2022) 151255, doi:10.1016/j.ejcb.2022.151255.
- [74] I.G. Gonçalves, J.M. Garcia-Aznar, Extracellular matrix density regulates the formation of tumour spheroids through cell migration, PLoS Comput. Biol. 17 (2021) e1008764, doi:10.1371/journal.pcbi.1008764.
- [75] S.J. Tan, A.C. Chang, S.M. Anderson, C.M. Miller, L.S. Prahl, D.J. Odde, A.R. Dunn, Regulation and dynamics of force transmission at individual cell-matrix adhesion bonds, Sci. Adv. 6 (2020), doi:10.1126/sciadv.aax0317.
- [76] A. Buttenschön, L. Edelstein-Keshet, Bridging from single to collective cell migration: a review of models and links to experiments, PLoS Comput. Biol. 16 (2020) e1008411, doi:10.1371/journal.pcbi.1008411.
- [77] B.A. Camley, W.-J. Rappel, Physical models of collective cell motility: from cell to tissue, J. Phys. D Appl. Phys. 50 (2017) 113002, doi:10.1088/1361-6463/ aa56fe.
- [78] Z. Yuan, Y. Li, S. Zhang, X. Wang, H. Dou, X. Yu, Z. Zhang, S. Yang, M. Xiao, Extracellular matrix remodeling in tumor progression and immune escape: from mechanisms to treatments, Mol. Cancer 22 (2023) 48, doi:10.1186/ s12943-023-01744-8.
- [79] C. Walker, E. Mojares, A. del Río Hernández, Role of extracellular matrix in development and cancer progression, Int. J. Mol. Sci. 19 (2018) 3028, doi:10. 3390/ijms19103028.
- [80] M.S. Hall, F. Alisafaei, E. Ban, X. Feng, C.-Y. Hui, V.B. Shenoy, M. Wu, Fibrous nonlinear elasticity enables positive mechanical feedback between cells and ECMs, Proc. Nat. Acad. Sci. 113 (2016) 14043–14048, doi:10.1073/pnas.